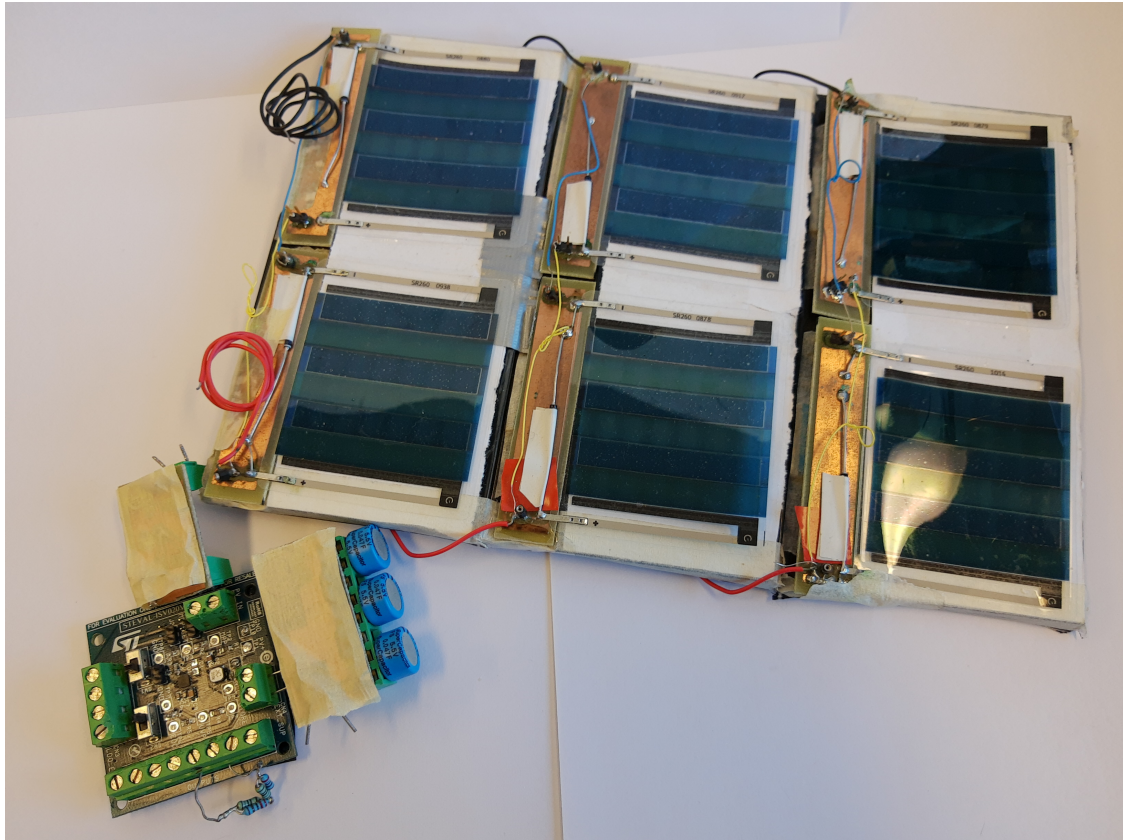




CHALMERS
UNIVERSITY OF TECHNOLOGY



Prototype of a sub-watt Light Energy Harvesting power solution

- For building sector monitoring equipment

Master's thesis in Electric Power Engineering

MARTIN GLIMSTRAND

DEPARTMENT OF ELECTRICAL ENGINEERING
CHALMERS UNIVERSITY OF TECHNOLOGY
Gothenburg, Sweden 2021
www.chalmers.se

MASTER'S THESIS 2021

Prototype of a sub-watt Light Energy Harvesting power solution

Martin Glimstrand



CHALMERS
UNIVERSITY OF TECHNOLOGY

Department of Electrical Engineering
Division of Electric Power Engineering
CHALMERS UNIVERSITY OF TECHNOLOGY
Gothenburg, Sweden 2021

Prototype of a sub-watt Light Energy Harvesting power solution
For building sector monitoring equipment
MARTIN GLIMSTRAND

© MARTIN GLIMSTRAND, 2021.

Supervisor: AXEL SJÖGREN HOLTZ, BRINJA
Examiner: TORBJÖRN THIRINGER, ELECTRIC POWER ENGINEERING

Master's Thesis 2021
Department of Electrical Engineering
Division of Electric Power Engineering
Chalmers University of Technology
SE-412 96 Gothenburg
Telephone +46 31 772 1000

Cover: Image of the completed prototype, consisting of light energy harvesting modules, power converter and capacitor bank.

Typeset in L^AT_EX
Printed by Chalmers Reproservice
Gothenburg, Sweden 2021

Prototype of a sub-watt LEH power solution in building sector monitoring equipment
MARTIN GLIMSTRAND
Department of Electrical Engineering
Chalmers University of Technology

Abstract

Recent developments in the fields of photo-voltaic (PV) and super-capacitors technology has enabled a wider range of products to be less reliant on the usage of batteries for electrical storage, or lessen the dependency on such solutions. A wide range of IoT products are now able to instead rely on useful power in the nearby environment through the use of devices known as 'energy harvesters'. Devices known as 'Light Energy Harvesting' (LEH) are able to extract useful power from light levels common to indoor environments, rather than intense sunlight. This thesis has created a prototype based on data collected on lighting conditions, temperature and humidity in building site conditions and combined it with LEH modules, an efficient DC/DC low power converter and super capacitors.

The prototype is able to supply useful power in ordinary in-door lighting conditions and the LEH module has been tested and been shown to work in a range of illumination from 120 to 1100 lux, temperatures between 7 and 31 degrees C, and been shown to be minimally impacted by humidity. The converter has been tested and shown to work well in illuminations ranging from 120 to 1100 lux with an efficiency of around 44%, producing between 1 and 5 mW. It is expected that with some additional work the prototype should be a viable supplement to the current power solution to current Brinja products. Some issues regarding the prototype and measurement set-up are brought up and future improvements are discussed.

Keywords: Power-converter, LEH, Super-capacitor, PV, MPP, Buck-boost converter, Energy storage.

Acknowledgements

I would like to thank my supervisor Axel Sjögren Holtz at Brinja and my examiner Torbjörn Thiringer for their time and support in making this thesis possible. I would like to thank my dear mother for her help and support. I would also like to thank Anton Lööf for his help in automatising my measurement setup, Christian Križan for his insights in the thesis work and David Johansson for providing essential parts for the setup. I would like to thank Felix Hulthén and Johan Karlsson for their help in proofreading my thesis. I would also like to thank Epishine for providing the LEH modules, ReVibe for their help in designing the power converter, and ETA for allowing me to use their space and equipment during the course of the thesis work. Lastly, I would like to thank everyone who lightened my burdens and brightened my days with their companionship through the thesis work and the testing times that have been. Without you this wouldn't have been possible.

Martin Glimstrand, Gothenburg, September 2021

Contents

1	Introduction	1
1.1	Background	1
1.2	Problem description	1
1.3	Aim	2
1.4	Limitations	2
2	Theory	3
2.1	Photo-voltaic cells	3
2.1.1	Photo-voltaic modelling	3
2.1.2	Optics	5
2.1.2.1	Illumination and chromaticity	5
2.1.3	LEDs	6
2.2	DC/DC conversion	6
2.2.1	Buck-Boost Converter	6
2.2.2	Background for MPP algorithms	7
2.2.3	The power converter IC	8
2.3	Super-capacitors	8
2.4	Humidification of air	9
2.5	Heat transfer	10
3	Case Set-up	13
3.1	Design of test chamber	13
3.1.1	Insulation of the test chamber	14
3.1.1.1	Atmospheric insulation of the test chamber	15
3.1.1.2	Thermal insulation of the test chamber	15
3.1.1.3	Optical insulation of the test chamber	15
3.1.2	Regulation of test chamber conditions	16
3.1.2.1	Usage of salts to regulate humidity	16
3.1.2.2	Usage of heat exchangers to regulate temperature	16
3.1.2.3	Usage of LED-strips to define lighting conditions	17
3.1.3	Placement of measuring equipment	19
3.1.4	Elimination of uncertainties	19
3.2	LEH setup and measurement	20
3.2.1	Measurement procedure	21
3.2.2	Measuring effect of long term humidity exposure	23
3.3	Digital load profile	24

3.4	DC/DC converter	24
3.4.1	Buck-Boost Converter Design	25
3.4.1.1	Implementation of Buck-boost converter.	25
3.4.1.2	Super Capacitor Board	27
3.4.2	Connectors and Test-points.	28
4	Results	29
4.1	DC/DC-converter	29
4.1.1	Resulting waveforms	30
4.1.2	Converter efficiency	31
4.1.2.1	Change of storage capacity	33
4.2	Test Chamber	33
4.2.1	True light distribution	33
4.2.2	PV power output depending on conditions	34
4.2.3	LED-strip illumination output temperature drift.	36
4.2.4	Long term humidity exposure on PV panels	37
4.3	Construction site lighting conditions	37
4.4	Prototype	38
4.5	Sustainability and ethics	39
5	Conclusion	41
5.1	Irregularities of the power converter.	41
5.2	Future improvements	42
A	Appendix 1	I

1

Introduction

1.1 Background

Over the last few decades massive improvements have been made to switch mode power supplies (SMPS) and photo-voltaic (PV) technology. The efficiency of these technologies are vastly improved and their increased power densities have enabled them to be found in ever smaller applications. PV technology has advanced to the point that viable in-door options are available, commonly known as Light Energy Harvesting (LEH), which are able to extract useful energy from ambient lighting conditions [1]. These conditions have been identified to be in the range of approximately 200-1000 lux [2]. This offers many new interesting possibilities in how energy is gathered and used, which may help in reducing future energy demands. The usage of super capacitors for sub-mW converter storage [3],[4] and the use of special techniques to get more useful energy out of capacitor storage [5] have been previously utilized to improve efficiency.

Construction has been identified as an area that constitutes a significant part of the global energy demand. Improvements in how energy is sourced may therefore be a great aid in the shift towards decreased reliability on non-renewable energy. By using a combination of SMPS and PV the possibility of creating wireless technology which doesn't require connection to the grid at all emerges. Brinja is a company which currently produces monitoring equipment solutions for construction sites and their ambition is to make them wireless and self-sustaining in order to make them more appealing on the market. By maturing the technology of in-door energy harvesting there may be future improvements in for example homes and office spaces in terms of their energy demand.

1.2 Problem description

In order to create a working prototype a viable indoor PV cell is required, as well as an efficient DC/DC power converter which is able to operate on low input power. Earlier work in these areas include clever ways of getting more usable energy from super capacitor storage, as well as efficient ways of performing power conversion for very small power levels [4]. These solutions have however not been performed in conjunction with LEH modules under varied conditions and thus leaves room for research into the subject. The PV cell will be tested on how climatic conditions such as temperature and humidity affects power generation, as well illuminance in

order to determine applicability during different lighting conditions. The DC/DC converter will be tested regarding its efficiency and ability to produce adequate power to the load under varying supply and energy storage conditions. These take the form of varying lighting conditions on the PV cell, and differing size and type of energy storage connected to the converter. The DC/DC power converter will additionally be tested over a varying temperature range.

1.3 Aim

The thesis aims to achieve the following:

- To create a prototype of a low power solution for sensor equipment based on the harvesting of indoor lighting using LEH technology.
- To evaluate the efficiency, applicability and viability of such a system by measuring energy harvesting potential under varying climatic and optical conditions.
- To evaluate the impact that the choice of energy storage has on efficiency and robustness of the system.

1.4 Limitations

Due to several limitations, though mostly time-constraints, some aspects of the thesis work which would contribute to results has to be omitted:

- The LEH modules will only be evaluated in a temperature span of 10°C to 30°C due to limited cooling and heating of the test chamber.
- The LEH modules will only be tested in lighting conditions similar to those expected in their later application.
- The DC/DC converter will not be implemented from scratch, but an evaluation board will be used instead.
- The chromaticity of the light source, and the chromaticity response of the examined LEH modules will not be examined.
- Only two levels of humidity will be examined.
- The final prototype will not be fully optimised for the expected conditions.
- A simplified model of the digital load will be used.

2

Theory

2.1 Photo-voltaic cells

PV cells are able to convert energy from photons into electrical energy through the photo-voltaic effect. Recent technological advancements have made it possible to harvest energy from indoor lighting. Modern PV cells are able to harvest $18 \mu\text{W}$ per cm^2 at an illumination of 500 lux [1]. Devices which are able to convert energy from different sources at very low energy densities are referred to as 'energy harvesters', while those who specifically do so using photons are called 'Light Energy Harvesters' (LEH).

2.1.1 Photo-voltaic modelling

In electrical systems a PV cell may be modelled as current source in parallel with a diode and an equivalent shunt resistance, as well as in series with a resistance [6], as shown in Figure 2.7.

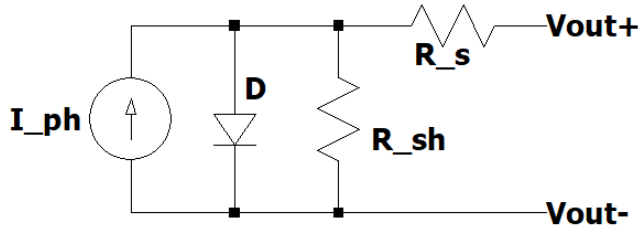


Figure 2.1: Single diode model of a PV cell, showing photocurrent I_{ph} , shunt-resistance R_{sh} , series-resistance R_s and internal diode D .

This model is commonly referred to as the "single diode model" of PV cells. In this model the amount of current produced by the current source is determined by how much light is striking the cell. The output current from a PV cell is

$$I_{out} = I_{ph} - I_s \left(\exp \left(\frac{q(V_{out} + I_{out}R_s)}{nkT} \right) - 1 \right) - \frac{V_{out} + I_{out}R_s}{R_{sh}} \quad (2.1)$$

where I_{ph} is the photocurrent, I_s is the the diode saturation current, q is electrical charge, R_s is the series resistance, n is the diode ideality factor, k is Boltzman's constant, T is the junction temperature, and R_{sh} is the shunt resistance [7]. (2.1) shows that the output current I_{OUT} of the PV panel is low for high values of V_{OUT} and vice versa. This also implies that the power produced by the PV panel should

2. Theory

be greatest somewhere inbetween these two extremes, where the product of the output current and voltage is the greatest [8][9]. This is shown in Figure 2.2. It may also be noted that the term $\frac{kT}{q}$ is also known as thermal voltage, and results in a voltage change depending on the temperature of the junction. The actual voltage change depends on several non-ideal effects and the value of the 'n' factor. The characteristics for the LEH module used are shown in Figure 2.3, including Short Circuit Current (SCC) and Open Circuit Voltage (OCV) [1].

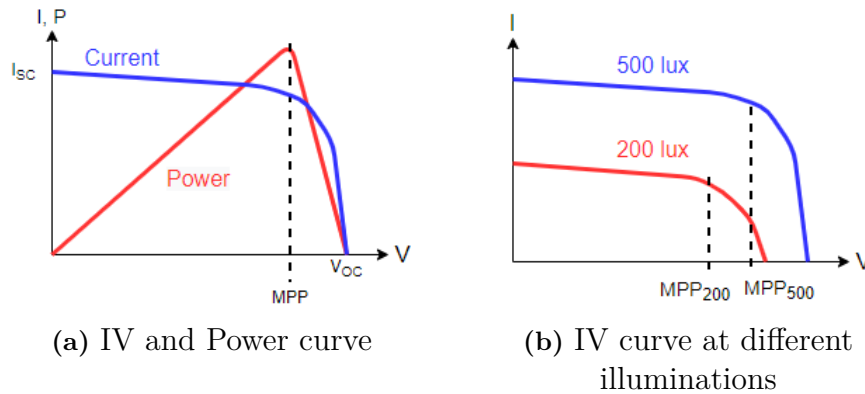


Figure 2.2: *Graphs showing where the MPP point is located, and how it changes depending on lighting conditions.*

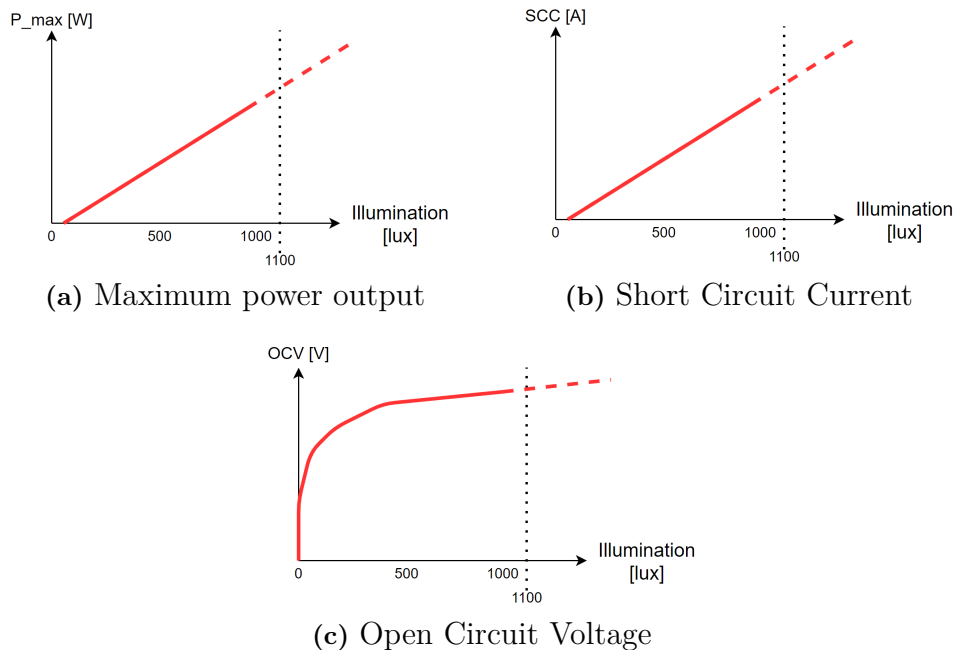


Figure 2.3: *Outline of maximum power, SCC, and OCV for the LEH module used depending on illumination from the datasheet, as well as extrapolated data used later. They are shown to be linear for maximum power and SCC, while being exponential for OCV.*

2.1.2 Optics

Light may interact with matter in three different ways. It may either pass through a material, be absorbed, or reflect off of it [10]. These three interactions between light and material are shown in Figure 2.4. The mode of interaction which takes place depends on the wavelength of light which falls onto the surface, but electrical energy is only created in PV cells when light is absorbed by the material [11]. Absorption of photons can only occur when the material has a band gap which is lower than energy content of a photon, at which point the excess energy becomes heat. Choosing PV panel material is therefore a trade-off between how much energy that can be absorbed and how efficiently this conversion takes place. PV panels which are designed for in-door use will therefore perform comparatively poorly in natural lighting conditions due to the difference in light intensity.

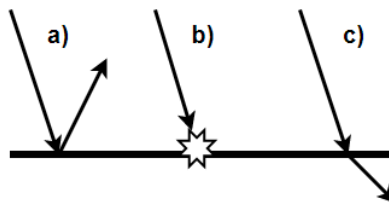


Figure 2.4: *Ways that light may interact with a material:*
a) Reflection, b) Absorption, c) Refraction

2.1.2.1 Illumination and chromaticity

When observing a light source modelled as a black-body object, the chromaticity of the light source may be described as a combination of colour and temperature and is usually how light sources are characterised. An illustration of the perceived temperature of a radiating object and its wavelength is shown in Figure 2.5 [12]. Illumination is a measure of the intensity of light which falls on an object, measured in lux.

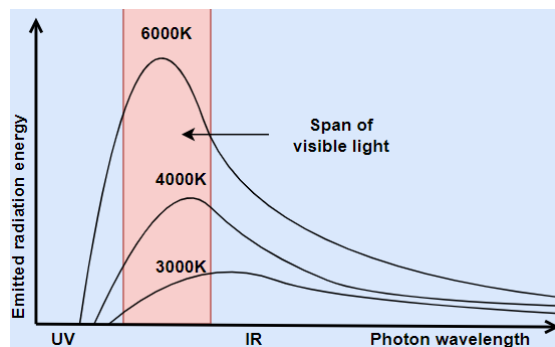


Figure 2.5: *Perceived colour of a black body radiating at a specific temperature.*

2.1.3 LEDs

Light emitting diodes (LED) do not distribute light evenly. Most manufacturers include a lens in front of the semiconductor which focuses photons in a desired direction [13]. This is characterised by the angle away from the center at which the light intensity has halved. This can be seen in Figure 2.6. This parameter is of interest when illuminating a surface, as it dictates at which distance the light source has to be placed and how densely they need to be installed in order to provide even illumination. This is further discussed in section 3.1.2.3.

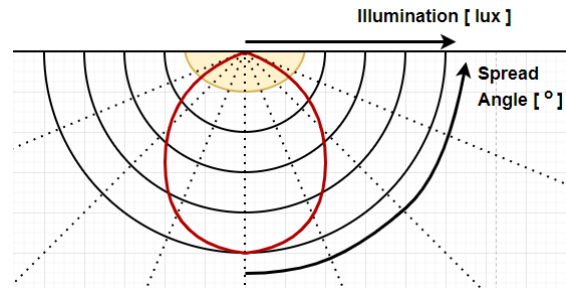


Figure 2.6: Example distribution of illuminance given off by an LED compared to the transmission angle at a set distance. The red line shows the characteristic illuminance distribution of the particular LED.

2.2 DC/DC conversion

The DC/DC power converter used for this prototype is based on the buck-boost converter typology [14]. This section will explore the working principle of the power converter and the additions made to it.

2.2.1 Buck-Boost Converter

The buck-boost converter is an inductor based power converter topology which uses a single switch to control power flow. The principal schematic of the buckboost converter is shown below.

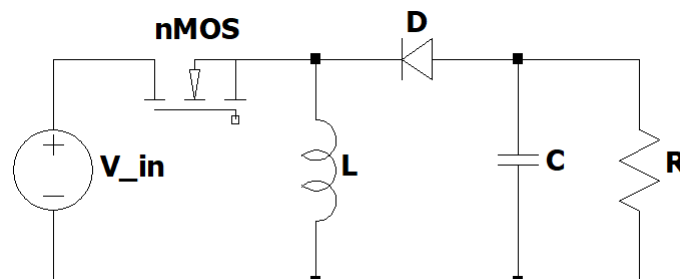


Figure 2.7: Schematic of the Buck-boost converter topology, showing the DC voltage input V_{in} , nMOS switch, inductor L , diode D , capacitor C and resistive load R .

Inductor based power converters store energy between switching cycles by creating a

magnetic field around the inductor which later collapses, transferring the energy to the circuit. The size of the inductor is based on the amount of energy that needs to be stored in-between cycles. This in turn depends on the load current and switching cycle according to:

$$L_{min} = \frac{V_i D}{I_{L,PP} f_s} \quad (2.2)$$

where L_{min} is the minimum required inductance, V_i is the input voltage, D is the duty cycle, $I_{L,PP}$ is the peak-to-peak current through the inductor, and f_s is the switching frequency [14]. The buck-boost converter is able to both step up and step down the input voltage by altering the duty cycle of the switch. The relationship between input and output voltage in an ideal buck-boost converter is given as

$$\frac{V_o}{V_i} = \frac{D}{1 - D} \quad (2.3)$$

where V_o is the output voltage, V_i is the input voltage, and D is the duty cycle of the switch. Due to parasitic elements present in the circuit this ratio is very inaccurate for large values of D because they result in a drop-off of the ratio between output and input voltage. The coulombic efficiency

$$\eta_{coul.} = \frac{P_{out} \cdot t}{P_{in} \cdot t} = \frac{V_{out} I_{out} \cdot t}{V_{in} I_{in} \cdot t} = \frac{E_{out}}{E_{in}} \quad (2.4)$$

2.2.2 Background for MPP algorithms

As shown in the Figure 2.2 there is a point at which the maximum amount of power is extracted from a PV panel, and that this moves depending on illumination. The Maximum Power Point (MPP) algorithm in the power converter controls operation in order to maximise output power as illumination and temperature on the LEH module changes. This is done by matching the equivalent impedance of the PV panels to the source impedance of the converter, as this is the point at which the most power is transferred. The SPV1050 does this in a static fashion by configuring resistors to operate close to the MPP of the PV panels at a single point [15]. This static configuration works well as long as the type of PV panel, amount of PV panels connected in series remains constant, and the light intensity which strikes the surface of the PV panels is somewhat constant. If the light intensity were to differ too much, the converter may produce much less power or even drop out due to too low input voltage. A more advanced version of this algorithm is the Maximum Power Point Tracking (MPPT) algorithm, which is able to dynamically change the operating point of the converter to match that of the power source in real-time [16]. The evaluation board used in this prototype doesn't support this feature.

2.2.3 The power converter IC

The SPV1050 [15] may be configured for a wide range of inputs and outputs and operates well for very low currents and has a built-in MPP algorithm. The IC was chosen because it supported all of these critical features on a single device, massively simplifying the prototype building process. The alteration of a few resistors, two capacitors and a single power inductor is all that's necessary to configure the converter. The specific component choices are discussed in Chapter 4.1, as well as some of the trade-offs brought up by the manufacturer. A figure of development kit is shown in Figure 2.8.

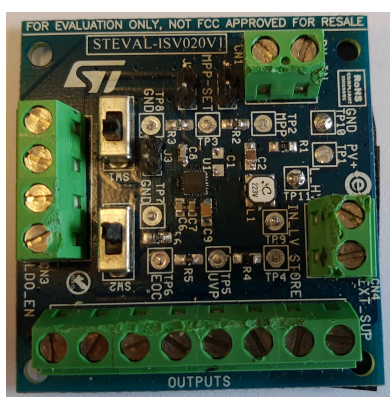


Figure 2.8: Picture of the ST evaluation board without any peripheral components.

2.3 Super-capacitors

Super Capacitors (SC), also known as 'Double layer capacitors' or 'Ultra capacitors' is a relatively new component on the market which offers new possibilities in electronics design due to their unique characteristics. Super capacitors offer very large capacitance values but only rated for low voltages as well as higher energy densities than electrolytic capacitors, and offers higher power densities than Lithium-ion batteries [17]. They also have very low series resistance, but also have relatively large leakage currents. This set of qualities makes super capacitors an appealing choice within IoT applications and other areas of low-voltage electrical power storage. Super capacitors are an appealing choice in small devices as they offer much higher energy and power densities for their volume than traditional electrolytic capacitors. This makes solutions much more compact and easily integrated in large systems. The super capacitors used are 'FS0H473ZF' made by Kemet [18]. They are rated for 5.5 volts and 47 mF each. A picture of this super capacitor is shown in Figure 2.9 as well as an electrolytic capacitor along with a comparison of their potentially stored energy.

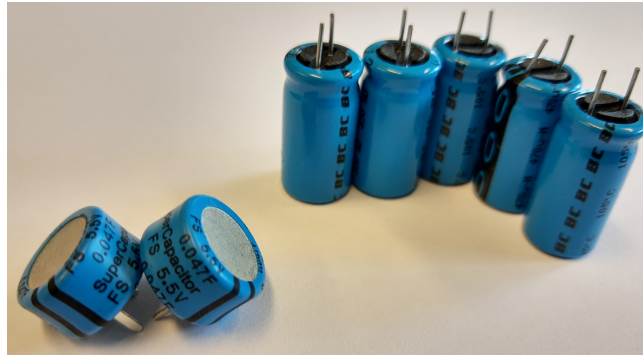


Figure 2.9: *The maximum rated energy of the two super capacitors on the left is equal to that of the five electrolytic capacitors to the right, but only needs a seventh of the voltage to do so.*

2.4 Humidification of air

In order to regulate the humidity in the test chamber different kinds of salts were used to ensure that different humidity levels would be kept at different testing temperatures. Salts retain different levels of moisture depending on the specific type used and the temperature at which they are kept [19]. By gathering sensor data from building sites a profile could be created which shows the correlation between ambient temperature and relative humidity levels to be expected. A table was then used to find salts which would be suitable to get a specific humidity level at the specified temperature. When the salts are placed in an environment with a differing relative air humidity, the water suspended in the air and within the salt will diffuse until the two are in equilibrium, illustrated in Figure 2.10. Diffusion takes place in three separate areas inside the test chamber.

- **Between salt and air:** On the boundary between the ambient air and salt crystals, water molecules may cross over from one to the other.
- **Inside the salt:** As water is released or absorbed through the surface of salt, water travels out from/in towards the center, in order to balance the osmotic pressure.
- **Throughout the ambient air:** Air will keep exchanging moisture with it's surroundings until the enclosed volume has reached equilibrium. Forced convection will distribute humidity more quickly.

All of these processes have associated time constants, resulting in delays between initial and final moisture content. The time constant inside of salt is much longer than at the interface between salt and air. The change in humidity transportation is therefore dependant on the gradient of moisture between salt and atmosphere and surface in relation to volume of the salt used. The more of the salt is directly exposed to the atmosphere, the quicker the rate of change.

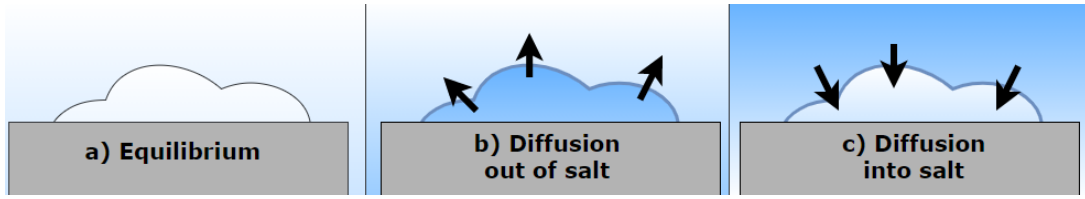


Figure 2.10: Diffusion of water between salt and ambient surrounding air. The net diffusion of water is zero in equilibrium.

2.5 Heat transfer

The transfer of heat energy occurs when heat is transported from a hotter region to a colder region. This energy may be transferred in one of three different ways [20][21]:

- **Convection.** This occurs when fluids move in order to distribute heat, such as air or water.
- **Conduction.** This occurs when a solid material conducts heat through itself. Metals are typically seen as good thermal conductors.
- **Radiation.** All materials which are hotter than absolute zero emit thermal radiation due to the movement of atoms.

These modes of heat transfer are illustrated in Figure 2.11.

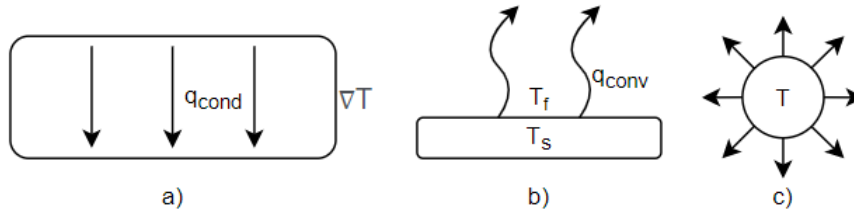


Figure 2.11: Illustration of how heat is transferred:
a) Conduction b) Convection and c) Radiation

Convective heat transfer may be described as shown in (2.5) at the interface between a solid and a fluid

$$q_{conv} = h(T_s - T_f) \quad (2.5)$$

where q_{conv} is convective heat transfer in $\frac{W}{m^2}$, h is the heat transfer coefficient in $\frac{W}{m^2K}$ which is dependant on the material, and T_s is the surface temperature of the solid and T_f is the temperature of the fluid at the interface. The convective heat transfer coefficient is a very complex variable which depends on velocity, surface area and much more. In general it is greatly increased with increased velocity. Similarly the conductive heat transfer across a temperature gradient over a solid medium may be described as in (2.6)

$$q_{cond} = k\nabla T \quad (2.6)$$

where q_{cond} is the conductive heat transfer in $\frac{W}{m^2}$, k is the conductive heat transfer coefficient of the material in $\frac{W}{m^2K}$, and ∇T is the temperature gradient across the material. A table of some relevant conduction coefficients [21] can be found in Table 2.1. Finally radiative heat transfer is determined by (2.7) [12]

$$P_{norm} = \mathcal{E}\sigma T^4 \quad (2.7)$$

where P_{norm} is radiated power in $\frac{W}{m^2}$, σ is the Stefan-Boltzmann constant which is approximately equal to $5.67037 \cdot 10^{-8} \frac{W}{m^2K^4}$, T is the temperature of the object, and \mathcal{E} is constant used to approximate the behaviour of non-black bodies, ranging from zero to one. Radiated power can be assumed to be negligible for most non-ideal black bodies at room temperature.

Table 2.1: List of a few thermal conductivity coefficients for different materials.

Material	Thermal Conductivity Coefficient [W/m*K]
Aluminium	≈ 100
PET	< 1
Styrofoam	$\ll 1$

3

Case Set-up

For an overview of the resolution and uncertainty of instruments used, as well as a list of where different aspects of the measurement are discussed, please refer to the Appendix.

3.1 Design of test chamber

A custom test chamber was made in order to conduct measurements under controlled conditions. The test chamber was designed to ease the regulation of the temperature, light levels and humidity that the LEH modules were exposed to during measurements. In order to contain an exact amount of water vapour the setup was put inside a plastic container with sealed openings and grease to seal the lid. Polystyrene panels were used to create a thermal barrier against the ambient environment, and dark plastic sheets provided additional blockage of light from the outside. In order to create the testing conditions a combination of heat exchangers, salts, a small electric fan and an LED array was used. These are illustrated in Figure 3.1 as well as shown in Figures 3.2 and 3.3 along with the necessary openings and other test equipment. The features and design are further elaborated on in this chapter.

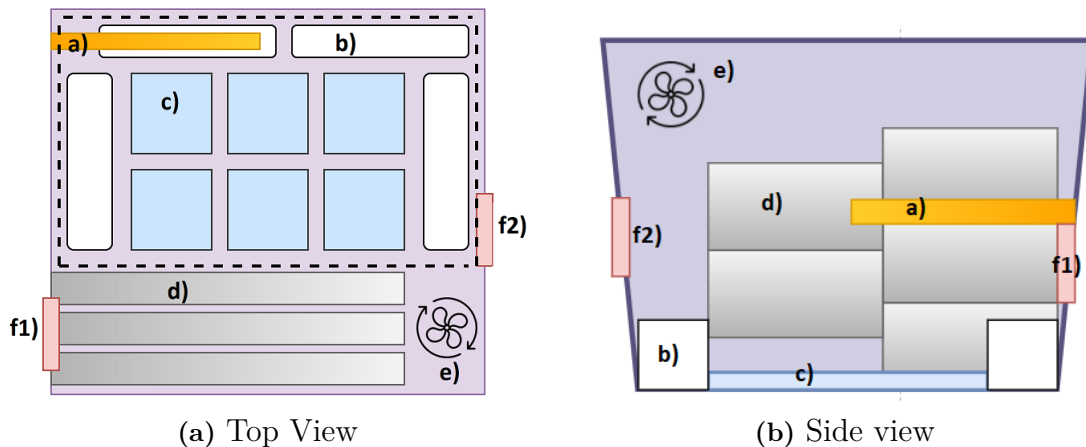


Figure 3.1: Test chamber interior showing: a) Measurement probe (gold), b) Salt containers (white), c) PV-panels (blue), d) Heat exchangers (gray), e) Fan, f1) Hosing exit (red), f2) Wiring exit (red). Dashed line encompasses area of direct illumination by LED-strips. Elements show relative position, not actual size.

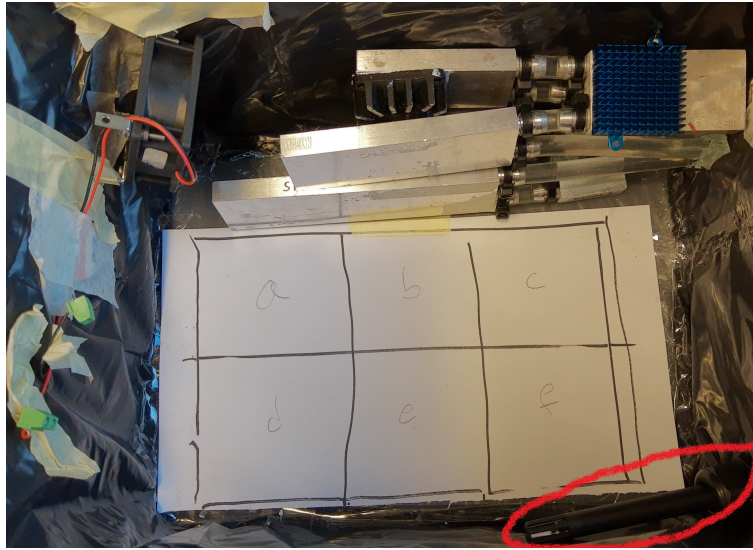
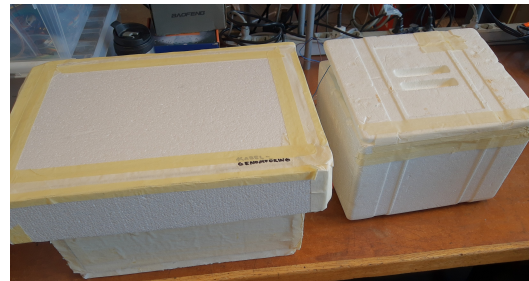


Figure 3.2: *Picture of the inside of the actual test chamber. Circled in red is the temperature/humidity probe.*



(a) Top side of test chamber lid



(b) Test chamber (left) and insulated water container (right)

Figure 3.3: *Pictures black acrylic panel containing LED-strips on the top side of test chamber lid and insulated box containing pump and water bath that were used during testing.*

3.1.1 Insulation of the test chamber.

A test chamber with minimal interference from its surroundings was needed in order to get reliable results. An exploded view of the different materials used to insulate the LEH modules inside the test chamber from light sources, heat and humidity in the air is shown in Figure 3.4.

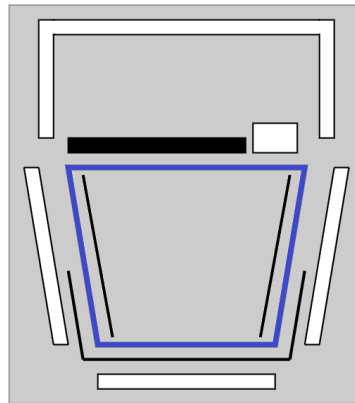


Figure 3.4: *Exploded view of the test chamber seen from the side showing the various kinds of insulation used. White parts are polystyrene, blue parts are plastic, thin black lines are black plastic sheets and the thick black lines is the acrylic plate with attached LED-strips.*

3.1.1.1 Atmospheric insulation of the test chamber

The chamber would need to be as close to airtight as possible in order to retain the correct amount of moisture during testing. A plastic storage container with a lid and clamps was used. Holes that were drilled into the sides of the container for hosing, wiring and the temperature probe were sealed using generous utilisation of a hot glue gun on both the inside and outside. In addition to this, the inside rim of the plastic lid had a layer of general purpose grease applied to it which would create an air tight seal when the lid was fastened to the box.

3.1.1.2 Thermal insulation of the test chamber

Because the test chamber needed to reach a significantly lower temperature than the ambient one during testing there was a need to provide thermal insulation in order to reach the desired temperature. This was done by encasing the plastic box in sheets of polystyrene. These sheets were placed on all four walls as well as the bottom. In addition to this a lid was created cover the top of the test chamber in order to further reduce the leakage of heat and can be seen in Figure 3.3. According to Table 2.6 we should expect that the rates of conduction from aluminium to air should be much higher than that of air to plastic, as well as through the polystyrene. This enables the heat exchangers to regulate efficiently no matter the outside conditions. Due to the poor grade of polystyrene, small cavities were present through which air could flow, reducing the insulating properties of the material. Masking tape was therefore used on the exterior of the polystyrene panels, as well as between the sheets of polystyrene, in order to trap more air and increase insulation.

3.1.1.3 Optical insulation of the test chamber

Due to the need of controlled lighting inside the test chamber there was a need to eliminate all sources of direct lighting of the test chamber, in addition to preventing as much of the indirect lighting as possible. This was achieved by all four walls

as well as the floor being covered in black plastic sheets which would absorb light which got through polystyrene walls. The LED-strips used to regulate the lighting inside the test chamber were mounted on a piece of black acrylic which provided some obstruction to outside light, as well as the polystyrene lid.

3.1.2 Regulation of test chamber conditions

3.1.2.1 Usage of salts to regulate humidity

Salts have the ability to dispense and absorb moisture to and from the environment. This ability can be used to create a stable relative air humidity inside an enclosed place. Different compositions of ions have varying ability to hold moisture, and this ability to retain moisture is also dependant on temperature [19]. In order to find appropriate salts a specific temperature and range of humidity was specified, and then a salt was chosen which fit these criteria, resulting in the salts chosen in Table 3.1.

Humidity is regulated by first measuring the ambient humidity of the room, and then proceeding in one of two ways depending on the results:

- If ambient relative humidity is higher than desired, the salts are first dried by heating them in a microwave oven in order to remove moisture content, then allowing them too cool in a sealed space, before being introduced to the chamber. In this way the salt is able to absorb excess moisture.
- If ambient relative humidity is lower than desired, the salts are introduced into a sealed chamber with a small amount of heated water. Once adequate time has passed the salts will have become saturated and are then introduced into the chamber.

It's very important to evacuate moisture from the chamber before experimentation, in order to not have excess moisture inside of the chamber. This will have the consequence of increasing the equilibrium point of the system. The expected relative humidity at different temperatures depending on the salt used is shown in Table 3.1.

Table 3.1: *Expected relative humidity from different salts depending on ambient air temperature at equilibrium.*

Temperature [°C]	10	15	20	25	30
NaOH [%]	-	9.57±2.8	8.91±2.4	8.24±2.1	7.57±1.7
K(CO3) [%]	43.14±0.39	43.15±0.33	43.16±0.33	43.16±0.39	43.17±0.5
KI [%]	72.11±0.31	70.98±0.28	69.90±0.26	68.86±0.24	67.89±0.23
KCl [%]	-	-	-	97.88±0.49	97.08±0.41

3.1.2.2 Usage of heat exchangers to regulate temperature

Heat exchangers made out of drilled out aluminium were used in order to regulate the temperature inside the test chamber. This was executed by pumping water through them until the chamber reached the desired temperature from a chamber insulated with styrofoam. The hosing from the heat exchangers were put through one of the chamber walls and connected to separate thermally insulated chamber,

consisting of a plastic tub placed inside of a polystyrene box, along with a lid. In order to aid in heating and cooling the chamber the heat exchangers were placed in a staggered fashion, some of which had heat sinks attached with a film of silicon paste for improved thermal contact, in front of a small fan which created forced convection. This greatly improved the rate of heat exchange and also distributed thermal energy more evenly inside the chamber, improving measurement reliability. The configuration of heat exchangers inside the chamber is shown in Figure 3.5.



Figure 3.5: *Picture of the heat exchangers inside the chambers, which are placed in a staggered fashion with attached heat sinks to increase convective cooling.*

The plastic tub contained a submersible water pump which would put water through the heat exchangers. The temperature of the bath was regulated by varying the amount of ice and water of different temperatures in order to achieve the desired temperature. The ice and water content was altered manually as needed. Pictures of the pump and the water chamber is shown in Figure 3.6.



(a) Water pump



(b) Water chamber

Figure 3.6: *Picture a) shows the inlet of the pump, as well as connected hosing. Picture b) shows the pump submerged in the water chamber and with test chamber hosing attached. Red paper has been added to aid in contrast.*

3.1.2.3 Usage of LED-strips to define lighting conditions

In order to provide a regulated and predictable source of light for experimentation LED-strips of a specified temperature were placed on top of the plastic lid used to provide atmospheric insulation. The type of LED-strip used was chosen based on being the same as those used on-site at most construction sites to provide interior

lighting, based on information provided by Brinja. These LED-strips run on rectified AC power taken from the electrical grid, and the amount of light produced by the LED-strips could be defined by varying the input voltage to the rectifier by the usage of autotransformer. In order to reduced the number of segments that needed to be soldered together and insulated, as well as to reduce the potential risk of failure of the LED-strip, the LED-strip was cut into one-meter segments and then folded and fastened onto a black acrylic plate using zip-ties. This had the issue of the strips needing to be bent and twisted in order to be placed as flatly as possible, resulting in less even light distribution at the ends of the acrylic panel. The idealised light distribution inside the chamber can be seen in Figure 3.7.

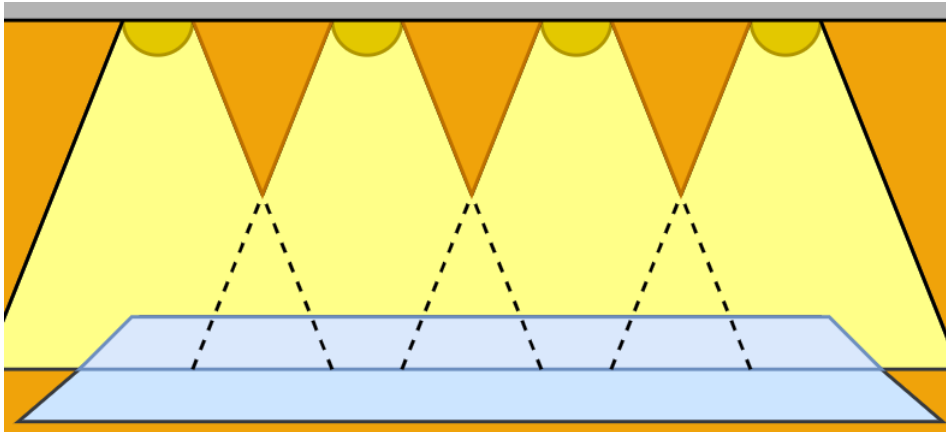


Figure 3.7: *Illustration of how light from adjacent LEDs on a strip illuminate a surface, showing overlapping cover.*

As can be seen in Figure 3.7 the idealised light distribution results in an overlap of emitted light coming from the ends of the plate, increasing illuminance there compared to the ends. This in turn is magnified by the ends of the one-meter LED-strip segments not being flush against the acrylic plate. In order to create a more even light distribution over the PV-panels pieces of paper were taped down in such a way that the ends recieved as much light as the middle. The LED-strip assembly and the placement of paper to block light can be seen in Figure 3.8. This was verified by measuring with the luxmeter in a grid replicating the placement of the panels. The LED-strips used were made by 'Tera Lite' and were rated to produce an equivalent temperature to that of a 3000 K blackbody, shown in Figure 2.5.

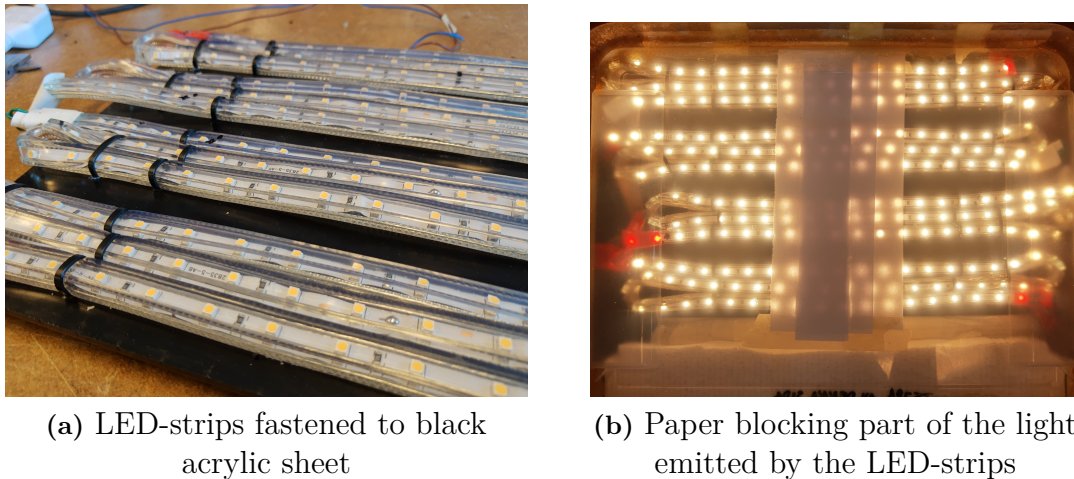


Figure 3.8: *Pictures of the LED-strip assembly, showing how they were mounted and how light distribution was later corrected.*

3.1.3 Placement of measuring equipment

The choice of plastic box, in addition to the required space needed for PV-panels and heat exchangers and salts, meant that there was very little space left to include other equipment inside the box, meaning that illumination could not be measured in real time. The probe [22] of the device used to measure the interior temperature and relative air humidity inside the chamber could be placed on one side without obstructing the solar panels from the LED-strips. The probe was placed on the opposite wall from the heat exchangers and a few centimeters off the bottom in order not get cooled or heated by the heat exchangers, thus creating less reliable readings. By installing a fan that blows air over the heat exchangers and through the chamber the probe would pick up a more reliable reading on temperature and moisture.

3.1.4 Elimination of uncertainties

In order to ensure that the results are as reliable as possible, as many unknowns as possible had to be eliminated while conducting measurements.

To make sure light emitted from the LED strips would vary as little as possible over time a 1 mF electrolytic cap was placed after the rectifier stage. This served the purpose of evening out the DC output voltage, creating a more even power flow to the LED strips. This also allowed for test points where voltage could be probed to ensure stable voltage on the output. Due to only having access to outlets where several other instruments and loads were connected the voltage supplied to the LED-strips were likely to be flattened and distorted as shown in Figure 3.9 a). This would result in an approximate voltage waveform as the one shown in Figure 3.9 b) being delivered to the LED-strips, which wouldn't be a perfectly smooth DC voltage.

The light distribution was observed before testing in order to make more even across the PV panel array. This was done by partitioning the area where the LEH module

3. Case Set-up

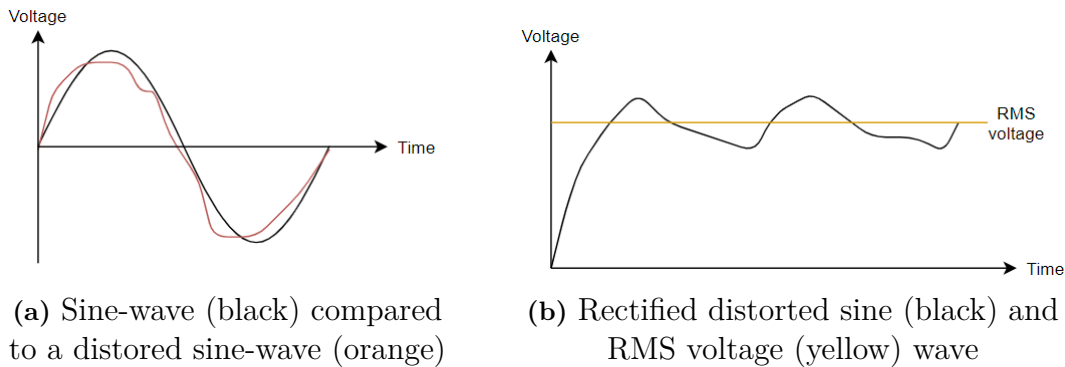


Figure 3.9: *Due to other loads on the power outlet, the sinusoidal voltage is distorted and results in an imperfect DC voltage being supplied to the LED-strips.*

array would be placed into six sections, corresponding to where the individual LEH modules would later be placed. A luxmeter was then placed in the center of these partitioned squares and the light intensity was then measured. The LED-strips were then partially covered up with strips of paper until the average light intensity of all squares would be close to equal to the light intensity at the square which was most easily measured. These measurements were done with the Styrofoam lid put on top in order to block as much outside light as possible.

Several tests were performed with salts and wet paper towels placed inside the chamber without the PV panel array being present in order to understand how the dynamics of temperature and humidity works. This mainly resulted in an understanding of how much salt needed to be used, how thinly it had to be placed in order to properly transpire, and how much time was needed for the system to stabilise. These experiments were also used to check for leaks in the chamber.

3.2 LEH setup and measurement

The indoor PV panels used in this thesis were supplied by Epishine, namely the 'LEH3_50x50_6_10' panels which produce $418 \mu\text{W}$ at 3.8 volts when exposed to 500 lux of direct light [1]. Six of these were placed into an array which could be easily be placed into and taken out of the test chamber while remaining flat and stable and is shown in Figure 3.10. The LEH modules were mounted on pieces of black acrylic which provided a flat base which the panels could be placed on and allowed for all panels to easily be moved together without shifting them relative to each other. The LEH modules were soldered onto PCBs with contacts to connect the modules to each other and reverse polarity diodes, whose forward voltage was measured to be 0.46 V, to avoid potential issues regarding dark spots on the panels. This can be seen in Figure 3.11 White pieces of ordinary office paper was also placed between the modules and the acrylic panels as per instructions from Epishine in order to increase efficiency.

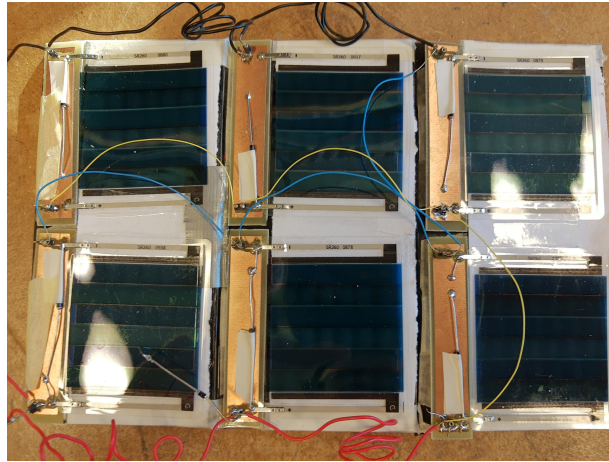


Figure 3.10: *The PV setup consisting of six LEH modules placed in parallel.*

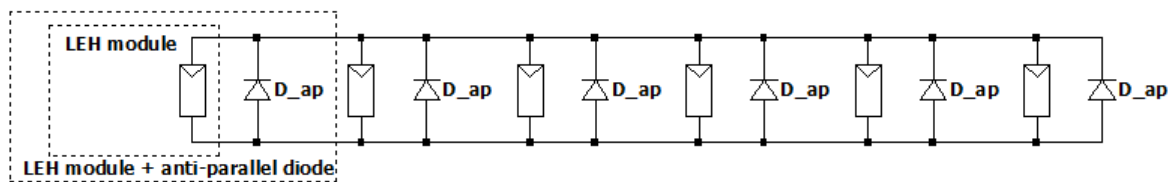


Figure 3.11: *Circuit diagram for six parallel LEH modules. The picture also shows the placement of anti-parallel diodes.*

By testing the PV panels under varying conditions such as different temperatures, humidity values and obstructions a better picture of real-world performance can be made. Humidity and temperature could be accurately recorded using the 'Testo 435' during testing, while Data collected by Brinja from work sites through their own sensor equipment provided general data on temperature, humidity and particles there. This data would be used to estimate the conditions the PV panels would be subjected to in those environments and evaluate their performance.

The datasheet for the LEH modules includes interpolated data points for illuminations ranging between zero and 1000 lux. Because the data acquired would range from zero to 1100 lux, the data had to be extrapolated to cover this setting. This was done by finding the slope of the maximum output power curve, dividing it by the linearly extrapolated OCV curve, which can be seen in Figure 2.3, resulting in an estimated maximum current. These values could then be compared against the measurements taken and thus be judged on their accuracy.

3.2.1 Measurement procedure

Measuring a full set of illuminations and temperatures for a given level of relative humidity took about four to five hours, in addition to the initial set up of all instruments. A picture of the measurement setup, including instruments, can be seen in Figure 3.13. The major steps taken before and during testing were as follows:

3. Case Set-up

1. Prepare a salt or wet paper towels in plastic containers and place inside the chamber to begin the process of bringing it to the right level of relative humidity.
2. Start the pump and bring the chamber temperature down to the lowest desired temperature of about 10 degrees.
3. When humidity and temperature are at the desired levels, begin the measuring process using the multimeters and Testo device. Record the current and voltage of the LEH module, as well as the temperature and relative humidity inside the chamber.
4. Go through all temperatures and light levels for the given level of relative humidity, making sure that the system reaches a steady state and that the DC voltage applied to the LED strips remains consistent between measurements.



Figure 3.12: *Picture taken of the average humidity test setup. From left to right on the table the laptop, cables, climate chamber, humidity+temperature sensor and Testo 435, water bath, and autotransformer can be seen. The PL303QMD power supplies and GW Instek multimeters can be seen on the shelf.*

A figure showing the most important parts of the electrical setup can be seen in Figure 3.13. An autotransformer allowed for a range of AC voltage inputs up to 300 volts. This voltage was then rectified through a full bridge rectifier and smoothed by a capacitor, producing a DC voltage similar to that shown in Figure 3.9. By toggling the MOSFET [23] on or off on the Arduino [24] board the SCC or OCV would be measured, respectively. This was executed by a script written in Python which communicated with both the Arduino and GW Instek multimeter, as well as saving their readings and states to an excel file which was used to record results. The voltage across the rectifier capacitor was also measured using a GW Instek.

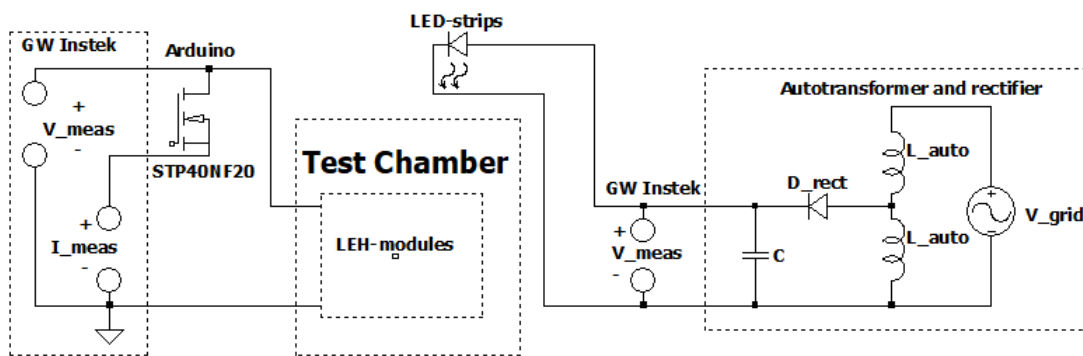


Figure 3.13: Simplified circuit diagram electrical system during testing. The appropriate voltage was set for the LED strip through the autotransformer and full bridge rectifier. The Arduino enabled the GW Instek to measure either voltage or current, as shown.

It should be noted that the transistor used on the Arduino introduces errors into the measurement in the form of a series resistance when conducting, resulting in a voltage drop across the transistor, as well as a leakage current when turned off which will be drained from the LEH modules. A few key values from the STP40NF20 datasheet are shown in Table 3.2. While the leakage current of the transistor can be assumed to be far below $1\mu\text{A}$, the $R_{DS,on}$ for a V_{GS} of 5 V wasn't provided in the data sheet.

Table 3.2: List of the most important parameters provided by the STP40NF20 datasheet. Because the area of operation was poorly defined exact numbers can't be provided.

Parameter	Conditions (Room temp.)	Value (typical)
$R_{DS,on}$	$V_{GS} = 10\text{ V}, I_D = 20\text{ A}$	38 m Ω
$V_{GS,th}$	$I_D = 250\ \mu\text{A}, V_{GS} = V_{DS}$	3 V
I_{leak}	$V_{GS} = 0\text{V}, V_{DS} = \text{MAX (rated)}$	1 μA

3.2.2 Measuring effect of long term humidity exposure

Before running tests with varying humidity levels two tests were run where the PV panels were exposed to a constant light intensity with the relative humidity would be as high as possible, and as low as possible. This would be run for a couple of hours in order to see if humidity would have a significant effect on short circuit current and open circuit voltage of the PV panels. The temperature was allowed to drift because the crude methods of temperature regulation would introduce too much uncertainty into the results, thus the temperature would increase as heat losses from the LED-strips and fan would accumulate.

The high humidity test done using paper towels placed upright in a trough of water. This allows for capillary action within the paper to increase the surface area of water to evaporate from, leading to an increased rate of evaporation. For the low humidity test Sodium Hydroxide powder was used to pull as much moisture out of the test chamber as possible.

3.3 Digital load profile

When creating a power supply solution the characteristics of the load need to be taken into account in order to make sure that enough power can be provided without damaging the device. When looking at IoT, sensors and other low power applications this becomes especially important as the small power levels creates large differences between the maximum and minimum power draw during normal operation. This mostly takes the form of different parts of the device consuming power at different points in time, and thus creating distinct pattern of power consumption depending on which function is being used.

The most important parts about the load profile are the

- Maximum variability in current draw.
- Average current draw.
- Delay between periods of large current draw.

Peak current draw from the converter is limited by the series resistance of the storage medium of converter, as this both slow down the ramp-up of current, causes increased heat losses, and limits the maximum current capability. Average current draw mostly determines the size of components and storage, as well as the number of PV panels which are needed. The delay between bursts of current draw affects the size of storage and power generation, as this will be the period in which power storage need to be refilled inbetween uses.

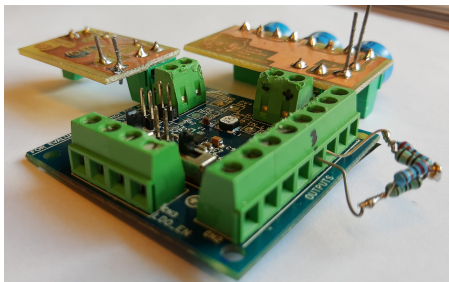
The load profile was measured using the "Energytrace" function in Code Composer Studio (CCS). This feature is able to record the power consumption, energy usage and current draw of digital equipment which it is connected to. The base power usage of the device was recorded by letting the load only perform base functions, which consisted in recording data from the installed sensors. Features such as communicating over WI-FI were turned off in order to establish a base line power draw for the device. This could then be compared to the power output of the PV panels to get an idea of excess power generation from the device.

3.4 DC/DC converter

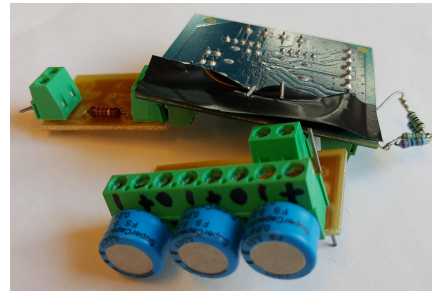
The main task of the power converter in the energy harvester setup is to provide a defined and stable output voltage, given a range of input voltages. This is most commonly done using either a boost or buck-boost topology and the choice comes down to system design. The buck-boost topology was chosen for the prototype because it enabled experimentation with a wider range of input voltages, and thus a greater freedom in design. ST offers a development for evaluation in energy harvesting implementations for the so called 'SPV1050TTR' buck-boost converter IC. The development kit saves a lot of time by not necessitating as much assembly and design on part of the user, as well as being more reliable than what could be created from scratch in the time frame of the thesis.

3.4.1 Buck-Boost Converter Design

In order to simplify the prototyping process the different parts of the circuit were assigned their own circuitboard, known as breakout boards. This technique was used in order to manufacture an accurate μA current-source, an adjustable super-capacitor bank, and an input circuit. Ease of measurement of the circuits was done in the form of test points which were easily accessible and allowed for probes to be moved away the central development kit board. The manufactured PCBs, as well as the converter, is shown in Figure 3.14.



(a) Side view of the DC/DC converter (middle) with attached external PCBs.



(b) Alternate view showing input PCB (left), SC bank (middle) and load (resistors).

Figure 3.14: Picture of the converter and load resistors, input resistor pcb and SC PCB attached. The exposed leads on the PCBs are the added test points.

3.4.1.1 Implementation of Buck-boost converter.

A simplified figure of the most important components relevant to the design of the development board is shown in Figure 3.15 and a table showing the accuracy of components used can be seen in Table 3.3

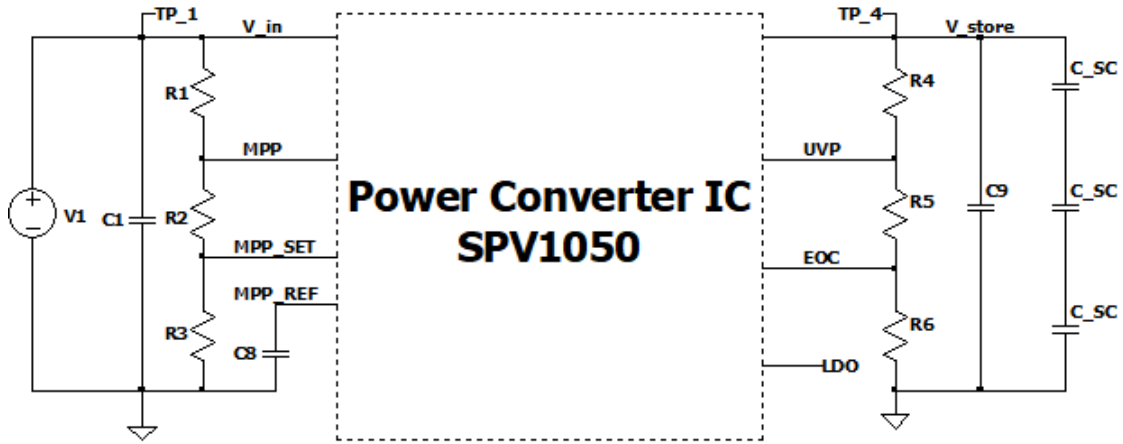


Figure 3.15: Simplified circuit diagram of some of the peripherals to the SPV1050 IC on the development board with the passive components and important voltages included. 'R' denotes resistors, 'C' denotes capacitors, ' C_{SC} ' denotes super capacitors as external storage, 'TP' denotes test points and the rest are voltages.

Table 3.3: Accuracy of the passive components used on the development board.

Component type	Resistors	Capacitors	Inductor
Accuracy	$\pm 1 \%$	$\pm 20 \%$	$\pm 20 \%$

A series of three resistors, R_1 , R_2 and R_3 together govern the voltage on the V_{MPP} , $V_{MPP-SET}$ and V_{UVP} pins of the converter. V_{MPP} is determined by

$$V_{MPP} = V_{in} \frac{R_2 + R_3}{R_1 + R_2 + R_3} \quad (3.1)$$

where V_{in} is the input voltage to the converter. This has to be equal or lower than V_{UVP} . V_{UVP} in turn is determined by

$$V_{UVP} \geq V_{oc,MAX} \frac{R_2 + R_3}{R_1 + R_2 + R_3} \quad (3.2)$$

where $V_{oc,MAX}$ is the maximum voltage that the LEH modules are able to produce. Finally in order to determine the configuration for the $V_{MPP-SET}$ voltage the MPP_{ratio} has to be determined, which is the fraction of the open-circuit voltage at which the source generates the most power. This fraction is defined as

$$MPP_{ratio} = \frac{V_{MPP-SET}}{V_{oc}} \quad (3.3)$$

Using Equation 3.3 we may define $V_{MPP-SET}$ as

$$V_{MPP-SET} = V_{in} \frac{R_3}{R_1 + R_2 + R_3} \quad (3.4)$$

In addition to these equations the current through the resistors must be negligible, making it so that the sum of resistors R_1 , R_2 and R_3 must be within the span of

10 M Ω and 20 M Ω . In order to calculate resistances R_4 , R_5 and R_6 we first establish the usage of an internal bandgap voltage which is defined as the following by the manufacturer

$$V_{BG} = 1.23 \quad (3.5)$$

This voltage is used to determine the threshold of the under voltage protection according to

$$V_{UVP} = V_{BG} \frac{R_4 + R_5 + R_6}{R_5 + R_6} \quad (3.6)$$

as well as the voltage at which to activate the end-of-charge state according to

$$V_{EOC} = V_{BG} \frac{R_4 + R_5 + R_6}{R_6} \quad (3.7)$$

In addition to these equations the current through the resistors must be negligible, making it so that the sum of resistors R_4 , R_5 and R_6 must be within the span of 10 M Ω and 20 M Ω . The input capacitor size is determined by the equivalent resistance, which depends on the voltage and current produced by the PV-panel. The converter uses this capacitor to sample the input voltage in order to operate the MPP function. The equivalent input resistance is determined by

$$R_{EQ} = V_{OC} \frac{(1 - MPP_{ratio})}{I_{MP}} \quad (3.8)$$

where R_{EQ} is the equivalent input resistance and I_{MP} is the current at the maximum power point. This resistance in addition to the input capacitance forms an RC-circuit which is charged during a 400 ms period that occurs every 16 s in which the capacitance is charged by the PV-panel while the converter is turned off. The time constant for this RC-tank is defined as

$$\tau = R_{EQ} C_{in} \quad (3.9)$$

where C_{in} is the input capacitance of the converter. This time constant must be chosen so that the capacitor is able to get as close to fully charged as possible within the allotted time frame when the converter is sampling.

3.4.1.2 Super Capacitor Board

Super capacitors may be damaged if soldered at too high a temperature, or for too long. Sufficient soldering temperatures and maximum soldering duration are provided by the manufacturer in their data sheet. To minimise this issue a breakout board was created where the capacitors were screwed onto screw terminals. A PCB was made so that up to three super capacitors could be placed in series. The total capacitance of capacitors connected in series is shown in (3.10). These equation shows that for equally sized capacitors connected in series the capacitance is divided by the total number of capacitors. The total energy stored in a capacitor bank can be calculated based on the total capacitance and rated voltage, as shown in (3.11).

3. Case Set-up

A table of the most important data for the super capacitor used can be seen in Table 3.4.

$$C_{ser} = \sum \frac{1}{\frac{1}{C_1} + \frac{1}{C_2}} \dots \quad (3.10)$$

$$E_C = \frac{1}{2} C_{tot} V^2 \quad (3.11)$$

Table 3.4: *Most important parameters for the type of super capacitor used.*

Product number	FS0H473ZF (KEMET)
Capacitance tolerance [%]	-20/+80
Rated capacitance [mF]	47
Resistance [Ω] (1 kHz)	40
Discharge Current [μ A] (After 30 mins)	710

When it comes the aging of super capacitors there are two main factors to examine: Temperature and State Of Charge (SOC). Generally, the aging progress more rapidly when the SC operates at higher temperatures, and higher states of charge [25]. As the SC used in this prototype are expected to operate mostly at room temperature $\pm 10^\circ$ and at around 70% SOC this shouldn't cause adverse effects on aging.

3.4.2 Connectors and Test-points.

When connecting multiple PCBs it's very important to reduce resistance as much as possible in order reduce losses, and good connections also reduce the impact of stray capacitance and inductance. This is especially important when operating with low currents. Screw terminals offer a reliable way of mounting parts together while also being detachable and keeping leads short, assuming that stranded wires are used. This is because the leads are able to be compressed when screwed, thus increasing contact area and reducing the risk of un-screwing and reducing resistance. The placement of test points on the development board are placed in such a way that the oscilloscope probe and earth connector easily form a loop above the board, leading to EMI issues when probing. Test points were added on the attached PCBs in such a way that the probe and earth could be oriented away from the development board.

4

Results

4.1 DC/DC-converter

The passive components which were mounted on the power converter are shown in Table 4.1 and 4.2. The resulting thresholds resulting from these choices are shown in Table 4.3

Table 4.1: Resistor values chosen for the converter.

Resistor	R_1	R_2	R_3	R_4	R_5	R_6
Value [$\text{M}\Omega$]	10	1	5.6	9.1	0.5	4.7

Table 4.2: Capacitor values chosen for the converter. C_{in} , $C_{MPP-ref}$ and C_{st} are ceramic capacitors while C_{ext} is from super capacitors.

Capacitor	C_{in}	$C_{MPP-ref}$	C_{st}	C_{ext}
Value [μF]	23	0.033	51	15'700

Table 4.3: Resulting voltage values based on the chosen resistors in Table 4.1

Voltage	V_{UVP}	V_{EOC}	V_{MPP}
Value [V]	3.38	3.74	1.51

Two of voltages in Table 4.3 were verified using a multimeter: V_{EOC} and V_{UVP} were verified by measuring the voltage across the external storage when it began and finished supplying the load, respectively. The measured voltages were found to be accurate to within a few tens of mV, the discrepancy expected to be caused by the relatively slow refresh rate of the multimeter used. Additional passive components were selected: An input-resistor to the converter was chosen to emulate the equivalent series resistance of the PV panel array depending on the equivalent illumination, as well as the equivalent load from the IoT device. The values are calculated using 3.8 and data taken from the Epishine datasheet for the LEH modules. These values are shown in Table 4.4

4. Results

Table 4.4: Other resistors used externally on the converter. $R_{PV-eqv.}$ is the equivalent resistance of the six parallel LEH modules when illuminated and $R_{Load-eqv.}$ is the average load of the IoT device.

Illumination [lux]	$R_{PV-eqv.}$ [k Ω]	$R_{Load-eqv.}$ [k Ω]
120	3.23	1.92
550	0.82	1.92
1100	0.45	1.92

4.1.1 Resulting waveforms

The voltage waveform in Figure 4.1 shows the voltage across the input terminals as the MPP function is running. During this period of about 300-400 ms the converter stops switching and allows the input capacitor to be fully charged up to the OCV. The voltage drop from the start of the new switching cycle to end of the previous cycle shows the integrity of the MPP_{REF} voltage stored on capacitor $C_{MPP-ref}$. A small change means that the correct MPP is maintained throughout the switching cycle, leading to improved power transfer. A measurement of the time constant was also performed to verify the absence of parasitic resistances. A list of expected and measured values are tabulated in Table 4.5.

Table 4.5: List of measured parameters and their expected values.

Parameter	Expected Value	Measured Value
V_{OC} [V]	3.80	3.80
ΔV [mV]	-	140
$T_{sampling}$ [s]	300-500	340
τ_{RC} [ms]	18.7	10.4

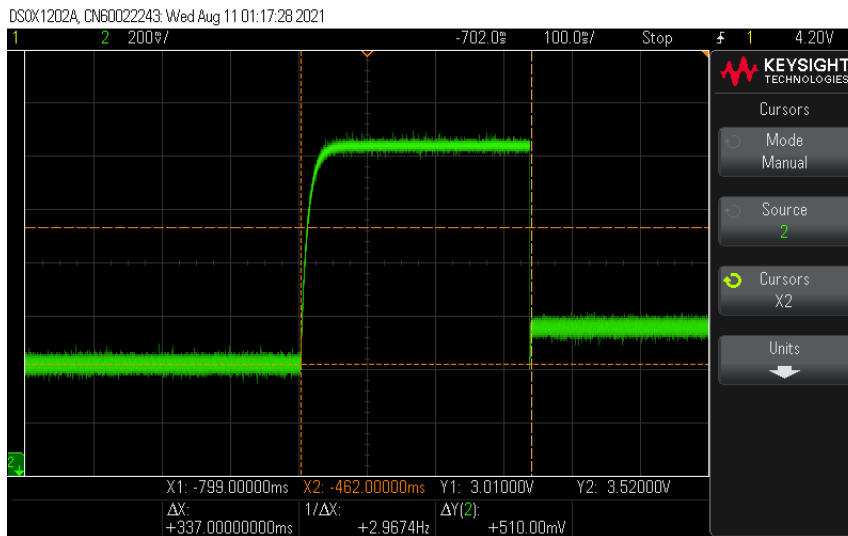


Figure 4.1: The picture shows the working of the MPP sampling algorithm on the converter input where the converter turns off briefly to detect the OCV. Note the change in voltage before and after the sampling of about 60 mV.

The voltage waveform in Figure 4.2 shows the voltage across the input terminals during incorrect operation, in this case when the external storage is three times that in Figure 4.1. Compared to the waveform in Figure 4.1 the ripple across the input capacitor is very large and the sampling time for the MPP function appears to be much shorter and to occur twice. Some suggestion on why this behaviour are brought up in the conclusions. The important aspect to bring up here is that the converter always behaves like this when starting from a completely discharged state, and usually performs normally after a few minutes.

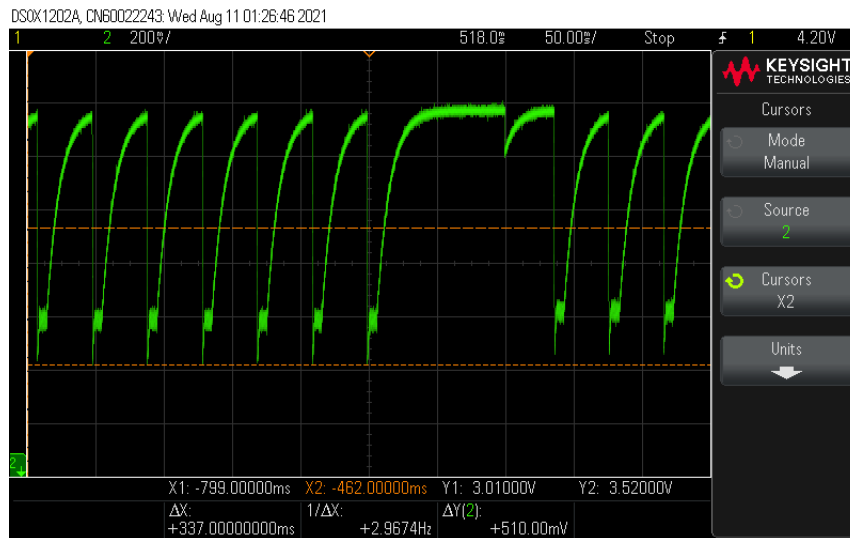


Figure 4.2: The picture shows the input voltage before the system has reached a steady state with a very large external energy storage. The sampling period here is only about 90 ms.

4.1.2 Converter efficiency

The coulombic efficiency of the converter at various illuminations of the LEH modules was examined to test resilience to changing conditions. This was done by supplying power to the converter through an equivalent input resistance using a 'PL303QM' DC power supply [26], while using the two available 'GW Instek GDM-8341' [27] to measure input and output power. The powersupply offers much more stable output than the LEH modules, which is why they were used for this test. The multimeters have a function which would allow them to sample up to 40 values per second, but this feature couldn't be properly implemented and thus a maximum of about 10 values a second could be recorded. In order to do this the multimeters were set up to record current and voltage respectively on either the input or the output, and would later be combined. This setup can be seen in Figure 4.3. The setup was allowed to reach steady state and then sampled for several periods of the external storage being charged by the input and then discharged through the load. This was done so that impact of variations in power intake from the MPP algorithm halting the converter, and power output due to the charging and discharging cycle, could be assumed negligible. The setup was allowed to run for approximately 15 minutes. The number of charge/discharge cycles, equivalent illumination and

4. Results

coulombic efficiency can be seen in Table 4.6

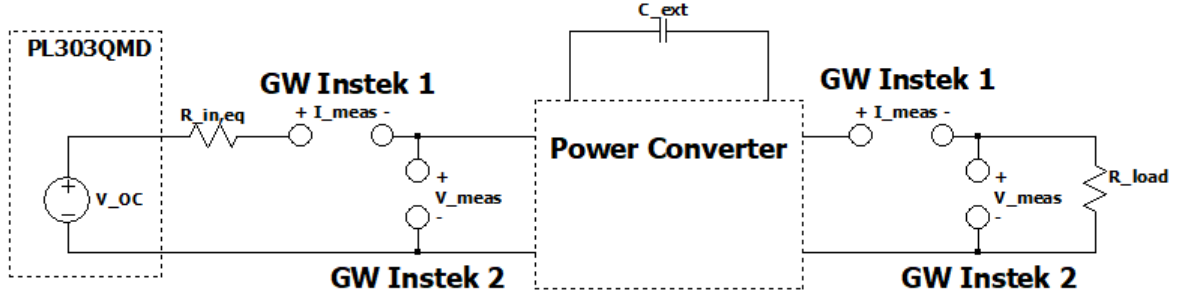


Figure 4.3: Diagram of the efficiency used to measure the efficiency of the converter, connected to a power supply and two digital multimeters to measure input and output power. The 'power'converter' shown is equivalent to the one seen in Figure 3.15.

Table 4.6: Equivalent illumination on the LEH modules and the resulting efficiency for the converter over a span of 15 minutes in steady state, as well as the Open Circuit Voltage (OCV) and equivalent input (R_{eq}) used.

Illumination [lux]	120	550	1100
Efficiency [%]	35	44	50
OCV [V]	3.63	3.95	4.1
R_{eq} [Ω]	3230	820	450

The need for a high sampling rate is to record the voltages and currents as accurately as possible. This is because the converter would only be able to sustain the output for a few seconds before hitting the EOC threshold, as well as the input shutting down power conversion for about 0.3 seconds every 15 seconds. Low sampling rates would lead to the calculated power being trapezoidal, rather than square, which is the actual behaviour of the output. This can be seen in Figure 4.4 where the difference in sampling rate and shape on sampled power can be seen.

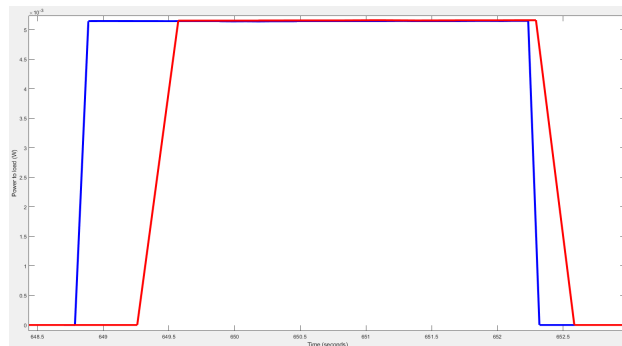


Figure 4.4: Graph of sampled power delivered to the load when two separate multimeters (blue) were used compared to one multimeter doing both (red) under identical conditions. Using one multimeter resulted in half the sample rate compared to using two, producing a distinct trapezoidal shape.

4.1.2.1 Change of storage capacity

Changes in the external storage capacity of the converter was examined for a single illumination in order to determine the impact of storage on the converter efficiency. A table of the equivalent resistance, storage size, and resulting efficiency can be seen in Table 4.7 as well as data for the individual super capacitors in Table

Table 4.7: Comparison of converter efficiency for two different values on the external super capacitor storage during identical conditions.

Equivalent Capacitance [mF]	R_{ESR} (1 kHz)	OCV [V]	R_{eq} [Ω]	Efficiency [%]
15.6	120	3.95	820	44
9.4	200	3.95	820	40

4.2 Test Chamber

The final test chamber was capable of reaching a minimum temperature of 8 °C after being chilled for 20 minutes in an ambient temperature of 23 °C. The lowest temperature the chamber was recorded to reach was about 6 °C and could go no higher than about 33 °C, due to the plastic hosing on the pump expand to such a degree that they dislodged themselves. The ambient illumination inside the chamber when the chamber was fully closed and LED strip was turned off was recorded to be between 1.5 - 4 lux, which is negligible compared the lowest used light setting during testing. The atmospheric was found to be sufficient, as the relative humidity of the chamber was able to reach very low levels and stay there for long durations.

4.2.1 True light distribution

Measuring the exact illuminance of the setup at the designated voltages was performed. The results using the Sefram luxmeter [28] are shown in Tables 4.8, 4.9 and 4.10 and are based on the grid shown in Figure 3.2

Table 4.8: Actual illuminance with the corresponding voltage shown in parenthesis.

115 (83,0)	123 (83,0)	117 (83,0)
118 (83,0)	117 (83,1)	121 (83,0)

Table 4.9: Actual illuminance with the corresponding voltage shown in parenthesis.

545 (108,1)	569 (107,6)	550 (108,1)
560 (108,0)	537 (107,9)	563 (108,1)

Table 4.10: *Actual illuminance with the corresponding voltage shown in parenthesis.*

1080 (138,0)	1153 (138.2)	1089 (138.0)
1111 (138,0)	1075 (138,0)	1113 (137,9)

Taking the mean across all squares shows the rough illumination for the whole PV array. The mean and maximum variation across all squares is shown in Table 4.11. These averages are referred to as being '120', '550' and '1100' lux in order to ease comprehension.

Table 4.11: Average illumination across all panels in the PV array, as well as the maximum difference across any two panels in the array at that setting.

Average Illumination [lux]	118	554	1103
Maximum Variation [lux]	8	32	73

4.2.2 PV power output depending on conditions

Of interest is the approximate power which the PV can deliver, depending on different conditions it may be experiencing. In Figures 4.5 and 4.6 the product of short circuit current (SCC) and open circuit voltage (OCV) is compared observed under varying lighting and humidity. It should be noted that the power levels are not the actual power which would be produced, only a useful metric to see the expected relative difference in produced power during these conditions. An overview of the SCC and OCV for various temperature and humidity values can be see in Figure 4.7.

It can be seen in Figure 4.5 that there is a strong linear correlation between the power product of the LEH module and the illumination in the chamber. This verifies the behaviour seen in Figure 2.3 a) from the manufacturer. According to equation 2.1 we expect to see a change proportional $exp(1/T)$ but the exact impact is difficult to determine. A comparison between the relative humidity and power product is shown in Figure 4.6 and shows that humidity has a negligible affect on the expected power output of the LEH module.

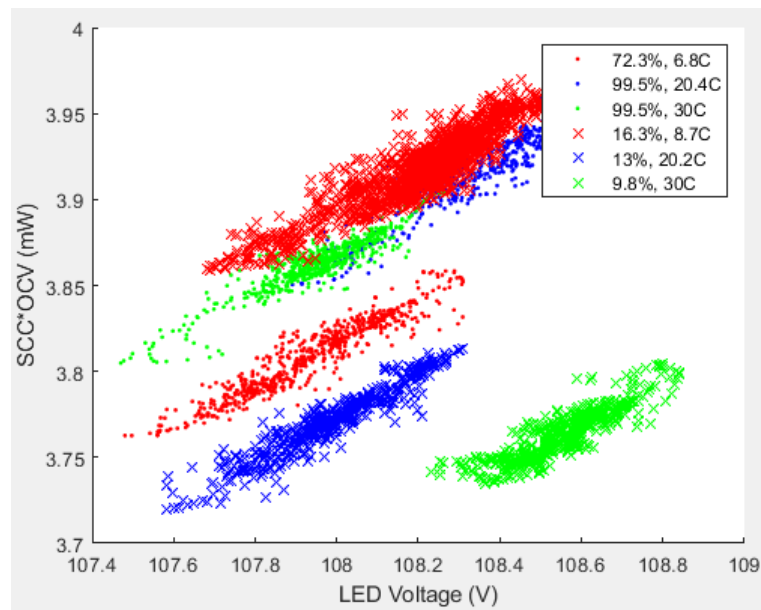


Figure 4.5: Plot of power product across a range of LED strip voltages. A strong linear correlation is observed.

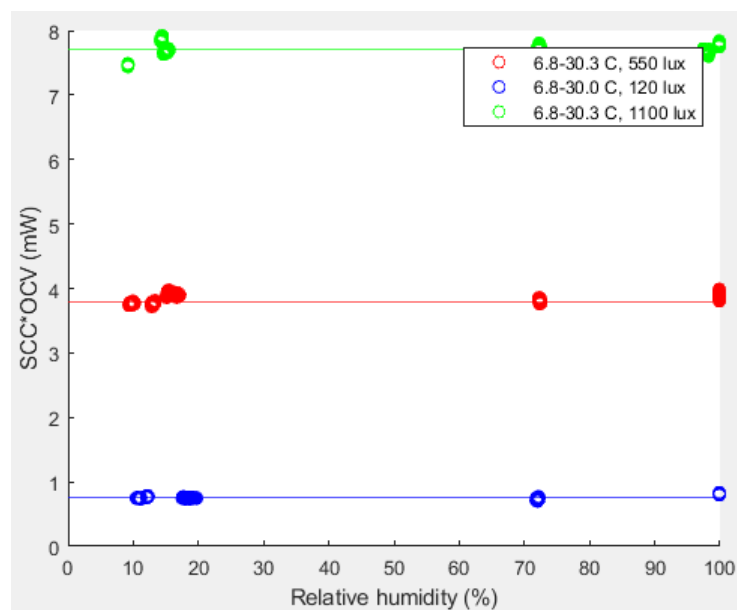


Figure 4.6: Plot of power product across a range of humidities. No significant correlation is seen.

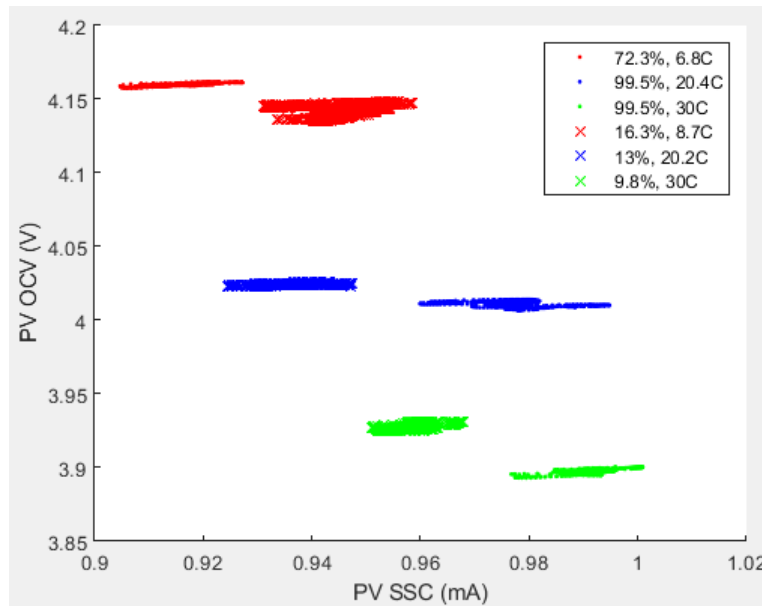


Figure 4.7: Plot of SCC and OCV for various temperatures and humidities at an illumination of 550 lux.

4.2.3 LED-strip illumination output temperature drift.

Because the chamber was too small to fit a luxmeter inside of it during testing the illumination had to be verified as being stable irrespective of the temperature inside the chamber. The result of an over one hour long test are shown in Figure 4.8. The chamber goes through a temperature change of about 18 °C while the humidity shifts around 45%. Because the change in voltage is too small to be seen at this scale a zoomed in view of the LED voltage as well as the measured illumination is provided Figure 4.9. It's apparent that illumination follows LED voltage very closely and doesn't drift as temperature increases, meaning that illumination can be assumed to be constant for all previous measurements.

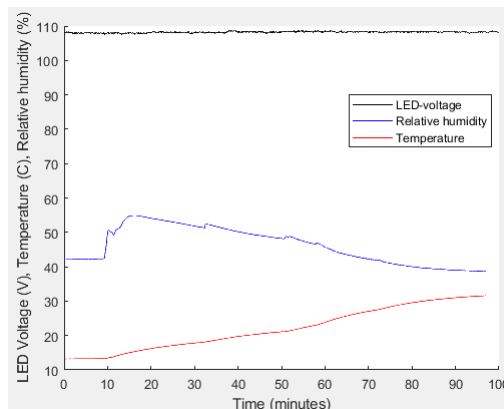


Figure 4.8: The temperature and relative humidity inside the test chamber and LED voltage during temperature drift test.

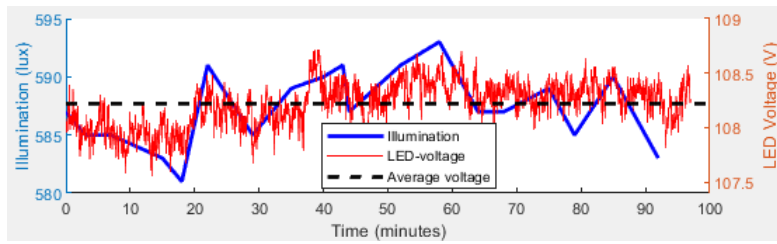


Figure 4.9: Zoomed in view of the voltage in Figure 4.8, as well as the measured illumination inside the chamber.

4.2.4 Long term humidity exposure on PV panels

The long term effects of humidity on the LEH modules is unknown. Two tests were performed where the modules were left in atmosphere of high and low relative humidity in order to verify that long term exposure wouldn't affect results. Before the dry test the LEH modules were placed into the climate chamber with sodium hydroxide salt for about 15 hours, and during about 18 hours with wet paper towels before the wet test. The results, when the effects of a difference in temperature between measurements and the interference of condensation is taken into account, doesn't show a significant difference in power output. The results can be seen in Figure 4.10.

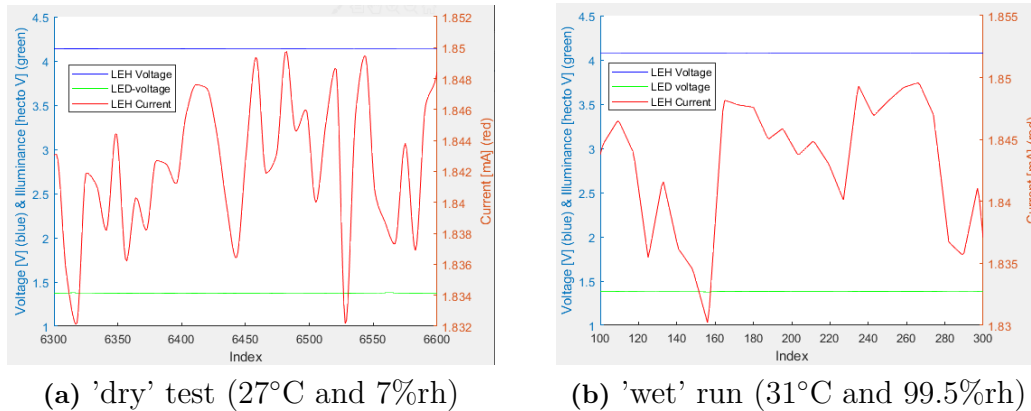


Figure 4.10: Comparison of LEH data after the panels being left to dry for 15 hours, and to soak up moisture for 18 hours. The voltage is 4.08V in a) and 4.135V in b).

4.3 Construction site lighting conditions

A visit was made to a construction site in Gothenburg in order to conduct measurements of lighting conditions inside the building. The building site had several cores and nodes installed by Brinja on several floors. The measurements were performed according to the variation in light levels, location inside the building, and where nodes had been installed. The visit was conducted between 16.00 and 18.00 on a

4. Results

sunny day with no clouds. A table of different areas and their estimated range of illumination is given in Table 4.12.

Table 4.12: *Measurements of ambient illumination conditions at a building site in different conditions.*

Location type	Range of illuminance [lux]	Expected suitability	Location example
(A) Dimly lit enclosed space	50 - 120	Very poor	Stairwell illuminated by a single vertical LED-strip
(B) Well lit enclosed space	150 - 300	Poor	Room illuminated by several LED-strip and/or LED bulbs in ceiling
(C) Dimly lit open space	350 - 500	Good	Room illuminated by some LED sources and distant reflections from sunlight
(D) Well lit open space	500 - 3000	Very good	Room mostly illuminated by reflections from sunlight
Sunlight through glass window	20 000 - 40 000	Acceptable	Floor and wall directly adjacent to glass window
Direct sunlight	80 000 +	Very Poor	Outside with no obstructions

The variation in illuminance seen in Table 4.12 depend on the orientation and distance of light armatures as well as that of the luxmeter as well as the reflectivity of nearby materials. The measurement data provided assumed a distance of about one to two meters from any particular light source and as an average of at least three different nearby location around the light source. This is the reason for the relatively dramatic change in light levels in location A) as compared location B) due to unevenness in light distribution.

Testing the light sources directly showed that they could create an illumination of about 500-1000 lux if the luxmeter was placed directly in front of the light source at a distance of about 30 centimeters. In rooms where sunlight was present, such as locations C) and D), the reflections evened out light distribution through the space, resulting in a tighter range of illuminance.

4.4 Prototype

A test was performed where the converter was connected directly to the LEH modules. The resulting power input to the converter from the LEH modules can be seen in Table 4.13

Table 4.13: *Resulting voltage, current, power, and stability of the LEH modules connected directly to the converter with three super capacitors. Stability is determined by if the circuit reaches the correct V_{OC}*

Illumination [lux]	V_{mpp} [V]	I_{mpp} [μ A]	P_{mpp} [μ W]	Stable
120	2.35	175	410	No
550	3.20	770	2460	Yes
1100	3.38	1480	5000	Yes

Since each panel is about 25 cm², and six of them were used in total, the resulting power density for the system will be as described in Table 4.14

Table 4.14: *The resulting power density of the prototype given total LEH module area of 150 cm²*

Illumination lux	P_{mpp} [μ W]	Power density [μ W/cm ²]
120	410	2.733
550	2460	16.4
1100	5000	33.33

4.5 Sustainability and ethics

The usage of LEH, as well as other types of energy harvesting technology, offer ways reducing the demand for more energy production by using energy which is already present but not fully utilised. If some form of energy harvesting is implemented into a product it offers an alternative to using energy from a power outlet which may be produced from fossil fuel sources, reducing environmental impact from everyday usage. It can therefore be concluded that depending on where this technology is used it may have major sustainability advantages compared to conventional solutions which are connected to the grid. The materials used in super-capacitors and those of the LEH modules are therefore of greater interest. Though specific materials used in the super capacitors and LEH modules are unknown, it is known that the super capacitors are covered by the RoHS directive. RoHS compliancy indicates that some chemicals and materials which are harmful to human and environmental health have been restricted in their usage [29]. These materials include lead, cadmium and mercury.

The usage of efficient power converters and the ability to work with very little power is of great importance as global electrical energy usage is quickly growing [], with a similar increase in environmental impact from electricity generation. Energy harvesting technologies therefore offer a way of generating more green energy in commercial products, while efficient devices reduce energy usage at the same time. This combination may provide an efficient and affable way to reduce environmental impact from a growing IoT industry sector in the future.

5

Conclusion

The thesis work has shown that it's possible to create a prototype for an IoT device used in constructions site conditions which is charged by LEH modules designed for indoor conditions based on lighting conditions, temperature and humidity. The converter was found to have an efficiency at around 44%, depending on the amount input power, and the SPV1050 MPP algorithm seems to work well for varying input power conditions. It was found that the effect of humidity and temperature on LEH module performance was minor compared to the level of illumination. The LEH modules appear to be unaffected by prolonged exposure to high and low humidity conditions. The LEH modules appear to be able to perform well in lighting conditions between 100 and 1100 lux. The full prototype was able to harvest about 1-5 mW from the LEH modules under the given conditions.

The prototype leaves room for improvement with regards to finer tuning of component choice on the development board to improve efficiency. It's believed that the relatively low degree of efficiency is due to many series connected capacitors, increasing series resistance, as well as flaws in PCB design and the absence of soldered connections on the super capacitors. The usage of a dedicated circuit, rather than usage of a development board and external circuit elements, would greatly improve performance and explains most of shortfall with regards to efficiency. It should also be noted that the usage of as few super capacitors as possible will improve performance.

5.1 Irregularities of the power converter.

There were many issues with the implementation of the power converter evaluation board. The primary issue was related to the soldering of components which caused current leakage issues. Due to the very low currents used by the power converter very large resistor values had to be used, which became bypassed by flux used when soldering. Though a solution was found, this flux residue may still decrease performance

The behaviour of the converter is not completely understood due to the data sheets for the device being difficult to grasp. The converter sometimes show the behaviour in Figure 4.2 instead of the desired behaviour shown in Figure 4.1. It has been discovered through changing some of the components on the evaluation board, as well as the number of super capacitors on the external storage, that this issue becomes rarer when:

- The external storage size is reduced.
- The inductor size is reduced.
- The input capacitor is reduced.
- The board is allowed to operate for a while.

This seems to indicate that the issue is related to the impedance that the converter is experiencing when operating. Inductor size correlates to DC current losses, meaning that keeping the inductor as small as possible will reduce losses, which was explained in the data sheet. By reducing the size of the capacitors on the input and external storage less energy was needed for the converter to find the OCV and the time needed to reach steady state operation, respectively. Due to a lack of directions on the sizing of critical components, other than to size them properly, it was difficult to size the system robustly enough to handle variations while operating efficiently.

5.2 Future improvements

There were several aspects of this thesis which negatively affected the quality of the data:

- During the high-humidity test it was observed that a lot of water vapour would condensate on the plastic lid separating the LED-strips and the PV array at higher temperatures. This would've effected the intensity of light reaching the LEH modules.
- Because the placement of the luxmeter and PV-array inside the chamber was done purely using visual aids, it's possible that they may have been misaligned between tests.
- The tests were originally supposed to be for three different temperatures, levels of humidity, and levels of illumination. Due to time shortage and degradation of the chamber itself this had to be reduced to only two levels of humidity, painting a less clear picture to draw conclusions from.
- The true 'temperature' of the LEDs used could not be verified, and the effects of using white office paper to block parts of the LED-strip on the LED temperature (as it absorbed some wavelengths) is unknown. Thus the precise illumination is unknown as the luxmeter couldn't be tuned in a meaningful way.

With regard to the measurement setup which was utilised in this thesis the most significant points are listed below:

- One of the most significant improvements which may be done is reduce the number of openings that need to be created to be as few as possible to reduce transfer of moisture between the test chamber and the outside. It should be possible to limit the amount of openings to two with the equipment which was used and thus more easily seal in the chamber.
- Using a test chamber with a larger footprint would also be preferable as this would allow for the use of more salts and measurements to be done simultaneously, allowing for light intensity to be monitored continuously and increasing the accuracy of data.
- Reducing the number of connections that need to be made to perform the measurements greatly reduces the time it takes to set up each experiment,

and greatly simplifies any troubleshooting process when something inevitably goes wrong.

- LED-strips should be implemented in such a way that as few gaps as possible introduced, evening the distribution of light in the chamber. Being able to selectively dim some LEDs near the middle further helps in evening the distribution of light. It may be preferable to choose a more opaque material to block out parts of the LED-strips

The above points show the importance of reducing the complexity of the measurement setup and to automate it in order to improve test result quality and data gathering speed. Using as few devices and instruments as possible is preferable to aid in solving issues. It is also to order many more different kinds of components, as well as more of them, when they are being purchased. This is in order to cut down on the impacts of lead time and not having spare components.

Finally, it would be of interest to future researchers to examine the impact that an MPP tracking algorithm would have on efficiency and applicability, as well as the impact of partially obstructing the PV panel array. The usage of reverse blocking diodes on each PV panel should minimise the negative impact of dark spots, as was done in this implementation.

Bibliography

- [1] Epishine. (Aug. 2021). “Epishine prouct page,” [Online]. Available: <https://www.epishine.com/product>.
- [2] M. Bass, *Handbook of Optics*, third. The McGraw-Hill Companies, 2010, vol. II, Chapter 40.7.1. [Online]. Available: <https://www.accessengineeringlibrary.com/content/book/9780071498906/chapter/chapter40>.
- [3] X. Yue, J. Kiely, D. Gibson, and E. M. Drakakis, “Charge-based supercapacitor storage estimation for indoor sub-mw photovoltaic energy harvesting powered wireless sensor nodes,” *IEEE Transactions on Industrial Electronics*, vol. 67, no. 3, pp. 2411–2421, 2020. DOI: 10.1109/TIE.2019.2896321. [Online]. Available: <https://ieeexplore.ieee.org/document/8673773>.
- [4] S. Kim and P. H. Chou, “Energy harvesting with supercapacitor-based energy storage,” in *Smart Sensors and Systems*, Springer, 2015, pp. 215–241. [Online]. Available: https://www.researchgate.net/publication/283801970_Energy_harvesting_Energy_harvesting_with_supercapacitor-based_energy_storage.
- [5] ———, “Energy harvesting by sweeping voltage-escalated charging of a reconfigurable supercapacitor array,” in *IEEE/ACM International Symposium on Low Power Electronics and Design*, IEEE, 2011, pp. 235–240. [Online]. Available: https://www.researchgate.net/publication/224254490_Energy_harvesting_by_sweeping_voltage-escalated_charging_of_a_reconfigurable_supercapacitor_arrayq.
- [6] D. Sinha, A. B. Das, D. K. Dhak, and P. K. Sadhu. (2014). “Equivalent circuit configuration for solar pv cell,” IEEE, [Online]. Available: https://www.researchgate.net/publication/271456027_Equivalent_circuit_configuration_for_solar_PV_cell.
- [7] H. Oudira, A. Mezache, and A. Chouder, “Solar cell parameters extraction of photovoltaic module using neider-mead optimization,” in *2018 IEEE 5th International Congress on Information Science and Technology (CiSt)*, IEEE, 2018, pp. 455–459.
- [8] P. Krzysztof (Kris) Iniewski, *Smart Grid Infrastructure & Networking*. McGraw-Hill Education, 2013, Chapter 5.14. [Online]. Available: <https://www.accessengineeringlibrary.com/content/book/9780071787741/chapter/chapter5#/ch05lev1sec14>.
- [9] P. H. Wayne Beaty Surya Santoso, *Handbook of Electric Power Calculations*, fourth. McGraw-Hill Education, 2015, Chapter 22.3.3. [Online]. Available: <https://www.accessengineeringlibrary.com/content/book/9780071823906/chapter/chapter22>.

- [10] M. Bass, *Handbook of Optics*, third. The McGraw-Hill Companies, 2010, vol. II, Chapter 35. [Online]. Available: https://www.accessengineeringlibrary.com/content/book/9780071498906/chapter/chapter35#/p200197b799735_7003.
- [11] —, *Handbook of Optics*, third. The McGraw-Hill Companies, 2010, vol. II, Chapter 25.
- [12] P. Keith J. Kasunic, *Optical Systems Engineering - Optical sources*. McGraw-Hill Education, 2011, Chapter 5 . [Online]. Available: <https://www.accessengineeringlibrary.com/content/book/9780071754408/chapter/chapter5#/ch05lev1sec01>.
- [13] M. Bass, *Handbook of Optics*, third. The McGraw-Hill Companies, 2010, vol. V, Chapter 13.9.1. [Online]. Available: https://www.accessengineeringlibrary.com/content/book/9780071633130/chapter/chapter13#/p200197ba99713_36001.
- [14] I. W. TI. (Aug. 2021). “Basic calculation of an inverting buck-boost power stage,” [Online]. Available: https://www.ti.com/lit/an/slva721a/slva721a.pdf?ts=1615291678415%5C&ref_url=https%5C%253A%5C%252F%5C%252Fwww.google.com%5C%252F.
- [15] ST. (Aug. 2021). “An4397 application note evaluation board for spv1050 ulp harvester (buck-boost architecture),” [Online]. Available: https://www.st.com/resource/en/application_note/dm00100185-evaluation-board-for-spv1050-ulp-harvester-buckboost-architecture-stmicroelectronics.pdf.
- [16] O. Lopez-Lapena, M. T. Penella, and M. Gasulla, “A closed-loop maximum power point tracker for subwatt photovoltaic panels,” *IEEE Transactions on Industrial Electronics*, vol. 59, no. 3, pp. 1588–1596, 2012. DOI: 10.1109/TIE.2011.2161254. [Online]. Available: <https://ieeexplore.ieee.org/document/5940223?tp=&arnumber=5940223>.
- [17] R. P. Deshpande, *Capacitors*. McGraw-Hill Education, 2015. [Online]. Available: <https://www.accessengineeringlibrary.com/content/book/9780071848565/chapter/chapter13>.
- [18] KEMET, *Fg0h103zf datasheet*. [Online]. Available: <https://api.kemet.com/component-edge/download/specsheet/FG0H103ZF.pdf>.
- [19] L. Greenspan, “Humidity fixed points of binary saturated aqueous solutions,” *JOURNAL OF RESEARCH of the National Bureau of Standards- A. Physics and Chemistry*, vol. 81 A, no. 1, Jan. 1977. [Online]. Available: https://nvlpubs.nist.gov/nistpubs/jres/81A/jresv81An1p89_A1b.pdf.
- [20] E. N. G. Y. I. Cho, *Handbook of Heat Transfer - BASIC CONCEPTS OF HEAT TRANSFER*. McGraw-Hill Education, 1998, Chapter 1. [Online]. Available: <https://www.accessengineeringlibrary.com/content/book/9780070535558/chapter/chapter1?implicit-login=true>.
- [21] Y. A. Ç. Mehmet Kanoğlu, *Energy Efficiency and Management for Engineers*, first. The McGraw-Hill Companies, 2020, Chapter 3.3.2. [Online]. Available: <https://www.accessengineeringlibrary.com/content/book/9781260459098/chapter/chapter3#/c9781260459098ch03lev1sec03>.

-
- [22] Testo, Aug. 2021. [Online]. Available: <https://www.testo.com/en-TH/humidity/temperature-probe/p/0636-9735>.
- [23] *Stp40nf20 datasheet*, ST. [Online]. Available: <https://www.st.com/resource/en/datasheet/stp40nf20.pdf>.
- [24] *Arduino mega 2560 datasheet*, Arduino. [Online]. Available: <https://store.arduino.cc/products/arduino-mega-2560-rev3>.
- [25] M. Ayadi, A. Eddahech, O. Briat, and J.-M. Vinassa, "Voltage and temperature impacts on leakage current in calendar ageing of supercapacitors," in *4th International Conference on Power Engineering, Energy and Electrical Drives*, 2013, pp. 1466–1470. DOI: 10.1109/PowerEng.2013.6635831. [Online]. Available: <https://ieeexplore.ieee.org/document/6635831>.
- [26] *Pl303qmd datasheet*, AIM & THURLBY THANDAR INSTRUMENTS, Aug. 2021. [Online]. Available: <http://www.farnell.com/datasheets/1733186.pdf>.
- [27] *Gw instek gdm-8341 datasheet*, GW Instek. [Online]. Available: https://www.gwinstek.com/en-global/products/detail/GDM-8342_GDM-8341.
- [28] *Sefram 9855 datasheet*, Sefram. [Online]. Available: https://bkpmedia.s3.amazonaws.com/downloads/datasheets/en-us/9855_datasheet.pdf.
- [29] *Rohs compliance*, European Commission. [Online]. Available: https://ec.europa.eu/environment/topics/waste-and-recycling/rohs-directive_en.

A

Appendix 1

Table A.1: Resolution and uncertainty for all instruments used

Instrument	Type	Range	Resolution	Uncertainty
GWinstek GDM-8341	Digital Multimeter	500 mV	10 μ V	0.02% + 4 digits
		5 V	100 μ V	0.02% + 4 digits
		500 μ A	10 μ A	0.05% + 5 digits
		5 A	100 μ A	0.05% + 4 digits
TTi PL303QMD	Linear Power Supply	30 V	10 mV	0.1% + 10 mV
		500 mA	100 μ A	0.3% + 0.3 mA
Testo 540	Lux meter	0-19999 lux	1 lux	± 3 lux or 3 %
Sefram 9855	Lux meter	40-40000 lux	-	± 6 %
Testo 435-2	Air Quality Meter	-25 to +74.9 $^{\circ}$ C	0.1 $^{\circ}$ C	0.2 $^{\circ}$ C
		100 %rh	0.1%	depends on probe
Testo Probe	Humidity/ Temperature Probe	-20 to +70 $^{\circ}$ C 100 %rh	-	0.2 $^{\circ}$ C

Table A.2: List of equipment used for the prototype, or the testing and evaluation of the prototype.

Item	Usage	Important information	Covered in section(s):
Submersible galley pump	Heating and cooling	Sold by Biltema (Art. 25-980)	3.1.2.2
LED strip	Light Source	LED strips made by Teralite	3.1.2.3
LEH3_50x50_6_10	Light Energy Harvester	In-door LEH made by Epishine	3.2
Arduino Mega 2560	Toggling of LEH module	Microcontroller used to toggle OCV/SCC made by Arduino	3.2.1
STP40NF20	N-channel MOSFET	Used on Arduino to short LEH modules	3.2.1
SPV1050TTR	Power Converter	Development kit made by ST	3.4.1.1
FS0H473ZF	Energy storage	Super capacitor made by KEMET	3.4.1.2

DEPARTMENT OF SOME SUBJECT OR TECHNOLOGY
CHALMERS UNIVERSITY OF TECHNOLOGY
Gothenburg, Sweden
www.chalmers.se



CHALMERS
UNIVERSITY OF TECHNOLOGY